NORMAL MODE INITIALIZATION

Roger Daley

National Center for Atmospheric Research*
Boulder, Colorado 80307, U.S.A.

---

* The National Center for Atmospheric Research is sponsored by the National Science Foundation.

ABSTRACT

In recent years, there has been increasing interest in the use of normal mode techniques in numerical weather prediction. Most of this interest has been generated by the success of these techniques when applied to the long-standing problem of the initialization of primitive equation models. However, the model normal mode methodology also has potential as a diagnostic tool for understanding the behavior of primitive equation models.

In the following sections, we will review recent developments in this field. We will progress logically through the construction of the model normal modes, their properties and their use in initialization procedures. We will also discuss the relationship of normal mode initialization to quasi-geostrophic theory and outline the concept of the slow manifold.

1. INTRODUCTION

Primitive equation models, unlike quasi-geostrophic models, generally admit high frequency gravity wave solutions, as well as the slower moving Rossby wave solutions. Although there are gravity waves in the atmosphere, they are generally of much smaller amplitude than the gravity waves which appear in primitive equation models. Since it is primarily the low frequency part of the flow which is of interest, model gravity modes are at best a nuisance and at worst can seriously compromise the forecast procedure. First of all, gravity waves generally require short computational timesteps; secondly, they can interfere seriously with very short period forecasts (< 12 hours); and thirdly, they can impair the precipitation and vertical motion calculations. Consequently, it is advantageous if they can be suppressed from PE model integrations.

Gravity wave oscillations arise primarily from initial imbalances between the wind and mass fields. These imbalances exist partially because the observed or analyzed mass and wind fields contain error and partially because the model equations do not exactly describe the atmosphere. Gravity wave oscillations can be controlled to some extent by the addition of time or space dissipation terms to the model equations. However, the primary way of suppressing gravity waves is by balancing the initial state through an initialization procedure.

Classical static initialization procedures such as the linear and non-linear balance equations and variational techniques have been widely used. Dynamic initialization procedures, in which the model equations are integrated forward and backward in time with large damping factors, have succeeded in suppressing many of the gravity waves. However, like the classical static techniques they have not worked well for the larger scales or in the tropics.

The use of model normal modes for initialization is attractive because the normal modes each have an associated frequency and one can, in principle, suppress only the high frequency gravity modes. Flattery (1970) developed an analysis/initialization procedure based on the Laplace tidal equations. Williamson (1976) and Williamson and Dickinson (1976) found the normal modes of the NCAR general

circulation model. Their initialization procedure simply set the initial amplitudes of the high frequency gravity modes equal to zero. This procedure was only partially successful because the initial projection of the non-linear and forcing terms of the equations onto these high frequency modes rapidly re-excited them. Machenhauer (1977) and Baer (1977) independently overcame this problem with non-linear normal mode initialization which took some account of the non-linearities. Their procedures have been applied to several different models with considerable success.

In the following sections, we will progress logically through the construction of the model normal modes, their properties and their use in initialization procedures. We shall then consider the relationship of normal mode initialization to quasi-geostrophic theories and outline the theory of the slow manifold. We shall then discuss unresolved problems with normal mode initialization and finish by briefly covering related applications of model normal modes in numerical weather prediction.

2. THE FORECAST MODEL

The first step in normal mode initialization is to find the free normal modes of the forecast model. (We shall distinguish between the free and forced normal mode problems, later.) The model we shall use here is a baroclinic primitive equations model in pressure coordinates. This is a slightly simpler model than the usual sigma coordinate model, but the derivation of the normal modes is virtually the same. The normal mode problem for a pressure coordinate model was first solved by Flattery (1967), but we shall use an approach similar to that of Kasahara and Puri (1980). The equations of motion, thermodynamic and continuity equations for this model are

$$\frac{\partial \underline{v}}{\partial t} + \underline{k} \times f\underline{v} + \nabla\Phi = R_{\underline{v}} \tag{1}$$

$$\frac{\partial}{\partial t}\frac{\partial \Phi}{\partial P} + \frac{R\,\gamma^{*}\omega}{P} = R_{\Phi} \tag{2}$$

$$\frac{\partial \omega}{\partial P} + \nabla\cdot\underline{v} = 0 \tag{3}$$

where

$$R_{\underline{v}} = -\underline{k} \times \zeta \underline{v} - \tfrac{1}{2}\nabla \underline{v}\cdot\underline{v} - \omega\frac{\partial \underline{v}}{\partial P}, \qquad (4)$$

$$R_{\Phi} = -\underline{v}\cdot\nabla\frac{\partial \Phi}{\partial P} - \frac{R\gamma'\omega}{P}.$$

$$\zeta = \underline{k}\cdot\nabla \times \underline{v},$$

$$\gamma = -\frac{T}{\theta}\frac{\partial \theta}{\partial P} = \frac{RT}{C_p P} - \frac{\partial T}{\partial P},$$

γ^* = horizontal average of γ, γ' = deviation,

R, C_p P, Φ are the gas constant, specific heat at constant pressure, pressure and geopotential,

$\omega = \frac{dP}{dt}$ and $\underline{k}$ is the vertical unit vector.

The vertical boundary conditions for this model are $\omega = 0$ at $P = 0$, and $w = \frac{dz}{dt} = 0$ at the ground ($z = 0$).

3. LINEARIZATION

The next step in generating the normal modes is to define a basic state and then linearize the model about it. We will define a very simple basic state - no flow and with a basic state static stability γ^* which is a function only of P. The structures and frequencies of the high frequency gravity modes are largely unaffected by the imposition of a more realistic basic state (see Kasahara, 1980). Since, in the initialization problem, it is the high frequency modes which are of primary concern, a basic state at rest is sufficient.

We shall write the model equations in spherical polar coordinates with the linearized terms on the left hand side and the non-linear terms on the right hand side:

$$\frac{\partial u}{\partial t} - 2\Omega \sin\phi\, v + \frac{1}{a\cos\phi}\frac{\partial \Phi}{\partial \lambda} = R_u \qquad (5)$$

$$\frac{\partial v}{\partial t} + 2\Omega \sin\phi\, u + \frac{1}{a}\frac{\partial \Phi}{\partial \phi} = R_v \qquad (6)$$

$$\frac{\partial}{\partial t}\frac{\partial \Phi}{\partial P} + \frac{R\gamma^*\omega}{P} = R_\Phi \tag{7}$$

$$\frac{\partial \omega}{\partial P} + \frac{1}{a\cos\phi}\left[\frac{\partial u}{\partial \lambda} + \frac{\partial}{\partial \phi} v\cos\phi\right] = 0 \tag{8}$$

where a = earth radius, Ω = earth rotation rate, λ, ϕ = longitude and latitude, and u, v = zonal and meridional velocity components. The linearized forms of the equations are obtained by setting $R_u = R_v = R_\Phi = 0$.

We can eliminate the variable ω by differentiating the linearized form of equation (7) with respect to P and introducing equation (8).

$$\frac{\partial}{\partial t}\frac{\partial}{\partial P}\frac{P}{R\gamma^*}\frac{\partial \Phi}{\partial P} - \frac{1}{a\cos\phi}\left[\frac{\partial u}{\partial \lambda} + \frac{\partial}{\partial \phi} v\cos\phi\right] = 0. \tag{9}$$

4. THE VERTICAL STRUCTURE EQUATION

We will now attempt to separate the horizontal and vertical dependence of the linearized equations (5, 6 and 9) by assuming that the dependent model variables u, v and Φ can be written as follows:

$$\begin{bmatrix} u \\ v \\ \Phi \end{bmatrix} = \begin{bmatrix} \hat{u}(\lambda, \phi, t) \\ \hat{v}(\lambda, \phi, t) \\ \hat{\Phi}(\lambda, \phi, t) \end{bmatrix} Z(P) \tag{10}$$

where Z(P) gives the vertical structure and $\hat{u}$, $\hat{v}$ and $\hat{\Phi}$ give the horizontal and temporal structure. Using the normal techniques of separation of variables, Eqs. 5, 6 and 9 (with $R_u = R_v = R_\Phi = 0$) can be written as three horizontal equations

$$\frac{\partial \hat{u}}{\partial t} - 2\Omega\sin\phi\,\hat{v} + \frac{1}{a\cos\phi}\frac{\partial \hat{\Phi}}{\partial \lambda} = 0 \tag{11}$$

$$\frac{\partial \hat{v}}{\partial t} + 2\Omega\sin\phi\,\hat{u} + \frac{1}{a}\frac{\partial \hat{\Phi}}{\partial \phi} = 0 \tag{12}$$

$$\frac{\partial \hat{\Phi}}{\partial t} + \frac{g\tilde{H}}{a\cos\phi}\left[\frac{\partial \hat{u}}{\partial \lambda} + \frac{\partial}{\partial \phi}\hat{v}\cos\phi\right] = 0 \tag{13}$$

and a vertical structure equation which is a function of P only

$$\frac{\partial}{\partial P}\left(\frac{P}{R\gamma^*}\frac{\partial Z}{\partial P}\right) + \frac{Z}{g\tilde{H}} = 0 \qquad (14)$$

where g is the gravitational constant, $\tilde{H}$ is called the equivalent depth and $(g\tilde{H})^{-1}$ is the separation constant. We note that Eqs. (11 - 13) are analagous to the linearized shallow water equations of a fluid with mean depth $\tilde{H}$, a fact first noted by Taylor (1936).

5. THE HORIZONTAL STRUCTURE EQUATION

The horizontal equations can be further separated by assuming an exponential behavior in time and longitude. Thus

$$\begin{bmatrix} \hat{u} \\ \hat{v} \\ \hat{\Phi} \end{bmatrix} = \begin{bmatrix} \hat{u}^m \\ i\,\hat{v}^m \\ 2\Omega\,\hat{\Phi}^m \end{bmatrix} \exp(i\,m\lambda - 2\Omega\, i\,\sigma\, t) \qquad (15)$$

where m is the zonal wavenumber, σ is a non-dimensional frequency and $i = \sqrt{-1}$. Substituting expansion (15) into Eqs. (11 - 13) gives

$$\sigma\,\hat{u}^m = -\sin\phi\,\hat{v}^m + \frac{m\,\hat{\Phi}^m}{a\cos\phi} \qquad (16)$$

$$\sigma\,\hat{v}^m = -\sin\phi\,\hat{u}^m - \frac{1}{a}\frac{\partial\,\hat{\Phi}^m}{\partial\,\phi} \qquad (17)$$

$$\sigma\,\hat{\Phi}^m = \frac{g\tilde{H}}{4\Omega^2 a\cos\phi}\left[m\,\hat{u}^m + \frac{\partial}{\partial\,\phi}\,\hat{v}^m\cos\phi\right] \qquad (18)$$

The elimination of $\hat{u}^m$ and $\hat{v}^m$ between Eqs. (16, 17 and 18) leads to the so-called horizontal structure equation

$$H(\hat{\Phi}^m) + \frac{4\Omega^2 a^2}{g\tilde{H}}\,\hat{\Phi}^m = 0 \qquad (19)$$

where

$$H = \left\{\frac{1}{\cos\phi}\frac{\partial}{\partial\,\phi}\left[\frac{\cos\phi}{(\sigma^2 - \sin^2\phi)}\frac{\partial}{\partial\,\phi}\right] + \frac{1}{(\sigma^2 - \sin^2\phi)}\left[\frac{m}{\sigma}\frac{(\sigma^2 + \sin^2\phi)}{(\sigma^2 - \sin^2\phi)} - \frac{m^2}{\cos^2\phi}\right]\right\}$$

is known as the horizontal structure operator.

Equation (14) - the vertical structure equation and Equation (19) are eigenvalue problems. The eigenvalue for the vertical structure

equation is $(g\tilde{H})^{-1}$ while the eigenvalue for the horizontal problem is the frequency σ. We shall distinguish here between the forced and free normal mode problems. In the forced problem, a forcing function and forcing frequency σ are imposed. In this case the horizontal equation (with σ specified) is solved to find the equivalent depth $\tilde{H}$ and then this $\tilde{H}$ is inserted in equation (14) to find the vertical structure.

It is the free normal mode problem which is of interest here. In the free case, the vertical structure equation is solved first to obtain a set of vertical eigenvectors each with associated equivalent depth $\tilde{H}$. We then have one horizontal eigenvalue problem to solve for each equivalent depth. In principle, with $\tilde{H}$ thus specified, we can solve the horizontal structure equation (14) obtaining a set of horizontal eigenvectors, each with an associated eigenfrequency σ. In practice, it is easier to solve the eigenvalue problem defined by equations (16 - 18) - which is equivalent to equation (19). This is because the eigenvalue σ appears in a complicated form in euqation (19).

6. BOUNDARY CONDITIONS

Before going on to discuss the solution of the vertical and horizontal structure equations, we must first discuss the spatial boundary conditions for these equations.

In the horizontal, we have assumed spherical polar geometry and there are no boundary conditions. In the case of a limited domain model, we would of course need boundary conditions for equations (16 - 18).

In the vertical, we need boundary conditions on Z at the top and bottom of the atmosphere. We will make use of the vertical boundary conditions discussed earlier, $\omega = 0$ at $P = 0$, and $w = 0$ at the ground.

At the top, we have from the thermodynamic equation (7) that

$$\frac{\partial Z}{\partial P} = 0 \quad \text{at } P = 0 \tag{20}$$

We can find the appropriate condition on Z at the ground as follows. We know that at the earth's surface (in the absence of topography)

$$w = \frac{dz}{dt} = 0$$

Linearizing and using the hydrostatic equation, we find

$$\frac{\partial \Phi}{\partial t} - \frac{\omega R T^*}{P_o} = 0$$

where P_o is the mean pressure at the ground, from which it can be shown that

$$\frac{\partial Z}{\partial P} + \frac{\gamma^* Z}{T^*} = 0 \qquad (21)$$

where T* = horizontally averaged temperature at the ground.

7. VERTICAL STRUCTURE FUNCTIONS

The vertical structure equation (14) and horizontal structure equations (16 - 18) are converted into algebraic eigenvalue problems by discretization. We shall concentrate on the discretization of the vertical structure equation, as it is more straightforward.

Most NWP models use a gridpoint representation in the vertical. Equation (14) with boundary conditions (21 and 22) would be solved using exactly the same vertical levels and finite-differencing used in the models. Imagine that the model uses 2nd order centered differencing and has L vertical levels with ℓ = 1, L ranging from the top to the bottom of the models. We would then find that equation (14) would have a finite difference representation for an arbitrary level ℓ as follows:

$$\frac{2}{(\Delta P_\ell + \Delta P_{\ell+1})} \left[B_{\ell+\frac{1}{2}} \frac{Z(\ell+1) - Z(\ell)}{\Delta P_{\ell+1}} - B_{\ell-\frac{1}{2}} \frac{Z(\ell) - Z(\ell-1)}{\Delta P_{\ell-1}} \right] + \frac{Z(\ell)}{g \tilde{H}} = 0 \qquad (22)$$

where

ΔP_ℓ = difference of pressure between levels,

$Z(\ell)$ = value of Z at level ℓ,

$B_{\ell+\frac{1}{2}}$ = $P_{\ell+\frac{1}{2}} / R \gamma^*_{\ell+\frac{1}{2}}$ and $\frac{1}{2}$ indicates half level.

All other levels would be similar except $\ell = 1$ and $\ell = L$ where the boundary conditions (20 - 21) would be used, This particular discretization is that used by Kasahara and Puri (1980). Other finite difference or finite element discretizations are given in Kasahara (1976), Daley (1979), and Temperton and Williamson (1979).

After discretization, equation (14) with boundary conditions (20 - 21) appears as the following algebraic eigenvalue problem:

$$\underline{\underline{A}}\,\underline{Z} + (g\tilde{H})^{-1}\,\underline{Z} = 0 \qquad (23)$$

where

$\underline{Z}$ is the column vector of $Z(\ell)$,

$\underline{\underline{A}}$ is the matriz of finite difference coefficients defined in equation (22).

Equation (23) can be solved by standard algebraic eigenvalue techniques to give L eigenvectors $Z_k(p)$, $k = 1$ to L, each with an associated eigenvalue (equivalent depth) $\tilde{H}_k$.

The vertical eigenvectors and associated equivalent depths for a typical atmospheric model (Kasahara and Puri, 1980) can be seen in Figure 1. There are 9 vertical levels and thus 9 eigenmodes. The vertical levels are indicated roughly as a function of P/P_o. The modes are ordered by decreasing equivalent depth. The gravest vertical mode (equivalent depth = 9750 m) is called the external mode, the others are called first internal, second internal, etc. The external mode has very little vertical structure. With decreasing equivalent depth the modes have more and more of their structure near the ground.

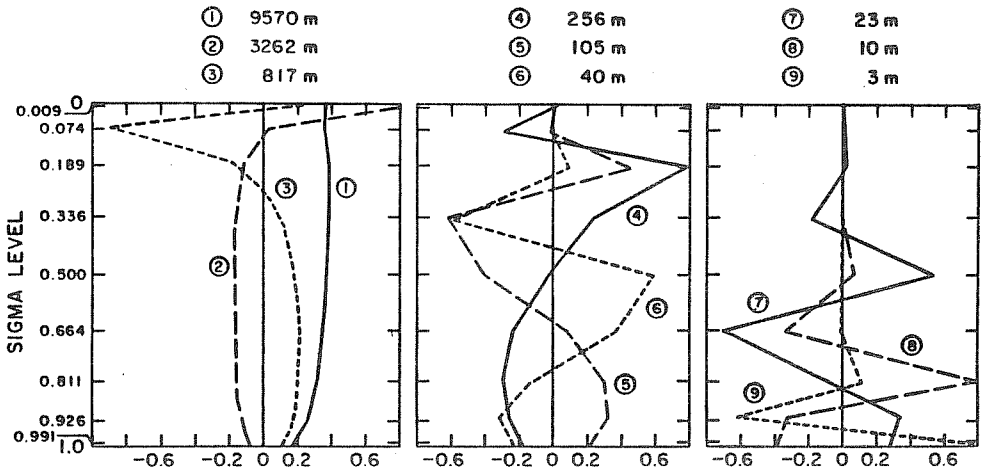

Figure 1 - after Kasahara and Puri (1980)

8. HORIZONTAL STRUCTURE FUNCTIONS

As mentioned in Section 5, the next step in the free normal mode problem is to take each of the L equivalent depths $\tilde{H}_k$, k = 1 to L, and solve the corresponding horizontal eigenproblem (19) or equations (16 - 18) for each $\tilde{H}_k$.

The horizontal eigenproblem can be turned into an algebraic eigenvalue problem by discretization. The traditional method for the spherical case is to expand the dependent variables in a spherical harmonic series. This leads to an algebraic eigenvalue problem for each zonal wavenumber. The solutions to this problem in the limit of an infinite spherical harmonic expansion are known as the horizontal structure functions or Hough functions (Hough, 1898; Longuet-Higgins, 1968). With each horizontal structure functions is an associated real eigenfrequency.

In the present case, however, we are attempting to find the free normal modes of atmospheric models which have only a finite number of degrees of freedom. Therefore, we are not interested in the actual Hough functions themselves, but discrete approximations to them.

In the case of a spectral model in which a truncated spherical harmonic expansion is used for the horizontal discretization, the horizontal structure functions would differ only slightly from the true Hough functions on the large-scale, but would differ appreciably on

the small scale. In the case of a finite difference model, a finite difference approximation consistent with the discretization of the model would be used in the discretization of equations (16 - 18). The resulting horizontal structure functions would again be similar to true Hough functions in the large scale, but differ for the small scale. For limited area models with lateral boundaries, there would also be boundary modes.

Let us suppose that our model has M zonal (east-west) degrees of freedom and N meridional (north-south) degrees of freedom. Thus, there are for each vertical mode k, MN horizontal degrees of freedom for each of the 3 dependent variables (u, v, Φ). Thus, there will be 3 MN horizontal structure functions for each vertical mode, each having a u, v, Φ component denoted below

$$\hat{u}_n^k(\lambda, \phi), \quad \hat{v}_n^k(\lambda, \phi), \quad \hat{\Phi}_n^k(\lambda, \phi) \quad 1 \leq n \leq MN$$

where n indicates the horizontal mode number. With each of the 3 MN horizontal structure functions is an associated eigenfrequency σ_n^k.

Now for the spherical case the modes can be classified by symmetry. In the symmetric case the modes $\hat{u}_n^k$, $\hat{\Phi}_n^k$ are symmetric with respect to the equator, while $\hat{v}_n^k$ is anti-symmetric. The symmetric modes would be the appropriate set for a hemispheric model. There is also an anti-symmetric set in which $\hat{u}_n^k$, $\hat{\Phi}_n^k$ are anti-symmetric while $\hat{v}_n^k$ is symmetric.

The horizontal structure functions can also be classified by their eigenfrequencies. There are basically two classes of modes. The first class consists of high frequency eastward and westward propagating gravity modes while the second class consists of low frequency westward propagating Rossby waves.

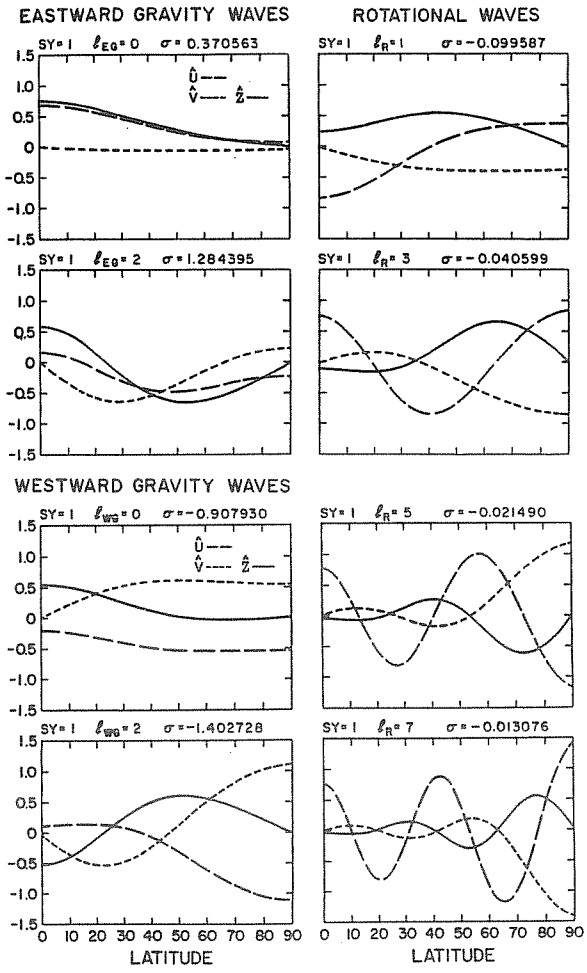

Figure 2 - after Kasahara (1976)

In Figure 2 is shown an example of meridional structure functions for zonal wavenumber m = 1 for the eastward and westward propagating gravity modes and the Rossby modes. The modes shown are all symmetric and the non-dimensional eigenfrequency σ is also indicated. The $\hat{u}$, $\hat{v}$, and $\hat{\Phi}$ structures are all shown. This figure from Kasahara (1976) shows the horizontal structure of true Hough modes, but one could imagine that the structure of these large-scale modes would not be much affected by discretization. The equivalent depth in this example is 10 km, corresponding to an external mode.

It can be noticed from Figure 2 that the magnitudes of the eigenfrequencies for the gravity modes are much larger than for the Rossby modes. For smaller equivalent depths, however, the absolute values of the eigenfrequencies for all modes tend to decrease. This effect can be seen in Table 1. In this table are plotted the non-dimensional eigenfrequencies for zonal wavenumber 1 for 2 equivalent depths, 10 km and .1 km. The frequencies of the 5 gravest symmetric gravity and Rossby modes are shown. The frequencies do not quite agree with those shown in Figure 2 because they correspond to the horizontal structure functions of the shallow water spectral model used by Daley (1978) which was rhomboidally truncated at wavenumber 31.

Table 1

Non-dimensional Eigenfrequencies

Zonal Wavenumber 1

10 km			.1 km		
Eastward Gravity	Westward Gravity	Rossby	Eastward Gravity	Westward Gravity	Rossby
.3693	-.9066	-.0994	.0339	-.3121	-.0112
1.2810	-1.3996	-.0406	.3246	-.4770	-.0049
1.9514	-1.9902	-.0215	.4833	-.5931	-.0032
2.6074	-2.6267	-.0131	.5980	-.6859	-.0024
3.2676	-3.2792	-.0087	.6903	-.7636	-.0019

It should be noted that some of the gravity modes for the .1 km equivalent depth have frequencies almost as small as the Rossby modes with equivalent depth 10 km.

For the spherical model, the Rossby modes for zonal wavenumber 0 are degenerate in that they have zero eigenvalues. Kasahara (1978) has considered this problem.

9. NORMAL MODE PROPERTIES

We will designate a particular normal mode using the following notation:

$$\hat{\Pi}_n^k(\lambda, \phi, p) = \begin{bmatrix} \hat{u}_n^k(\lambda, \phi) \\ \hat{v}_n^k(\lambda, \phi) \\ \hat{\Phi}_n^k(\lambda, \phi) \end{bmatrix} Z_k(P) \tag{24}$$

for each $\tilde{H}_k$ and eigenfrequency σ_n^k.

The $\hat{\Pi}_n^k$, being solutions to a linear problem, have an arbitrary amplitude. They are orthogonal, however, and can be normalized. We will write the orthonormality condition using inner product notation.

$$\langle \hat{\Pi}_n^k \cdot \hat{\Pi}_\ell^j \rangle = \delta_k^j \quad \delta_n^\ell \tag{25}$$

where δ_j^k is the Kronecker delta. Equation (25) follows from the fact that the horizontal and vertical structure functions are individually orthogonal. Thus

$$\int_P Z_k(P)\, Z_j(P)\, dP = \delta_k^j \tag{26}$$

$$\int_\lambda \int_\phi \left[\frac{g\tilde{H}_k}{4\Omega^2}\left(\hat{u}_n^k\ \hat{u}_\ell^k + \hat{v}_n^k\ \hat{v}_\ell^k\right) + \hat{\Phi}_n^k\ \hat{\Phi}_\ell^k\right] \cos\phi\, d\phi\, d\lambda = \delta_n^\ell$$

We have written these orthogonality conditions as if the vertical and horizontal structure functions were analytic. In general, these structure functions will only be defined at gridpoints and equations (25 and 26) would be replaced by numerical quadrature expressions consistent with the model discretization.

Let us define Π to be a vector of arbitrary wind and geopotential fields

$$\Pi = \begin{bmatrix} u(\lambda, \phi, P) \\ v(\lambda, \phi, P) \\ \Phi(\lambda, \phi, P) \end{bmatrix} \tag{27}$$

Then Π can be expanded in a series of normal mode functions in the same way one expands a field in a Fourier series. Thus

$$\Pi = \sum_n \sum_k x_n^k\, \hat{\Pi}_n^k(\lambda, \phi, P) \tag{28}$$

where

$$x_n^k = <\Pi \cdot \hat{\Pi}_n^k> \tag{29}$$

x_n^k is called the normal mode expansion coefficient. It can be obtained in equation (29) by projecting the data (u, v, Φ) onto the horizontal and vertical structure functions appropriate to that mode and making use of the orthonormality conditions (26).

10. NORMAL MODE FORM OF MODEL EQUATIONS

We can use equation (29) to write the linearized form of the model equations (5 - 8) in normal mode form. Thus, with $R_u = R_V = R_\Phi = 0$, we have

$$\dot{x}_n^k + 2\Omega i\, \sigma_n^k\, x_n^k = 0, \quad \text{all } k, n \tag{30}$$

where x_n^k is the expansion coefficient corresponding to the normal mode defined by (kn, n). This equation is produced from the linearized form of equations (5 - 8) simply by multiplying by the appropriate horizontal and vertical structure functions and integrating over the atmosphere as in equation (28).

Let us define X to be the vector of all normal mode expansion coefficients, i.e. each x_n^k is a member of X. Our real goal, here, is to find the normal mode form of the full non-linear equations (R_u, R_V, $R_\Phi \neq 0$). Let us define R_Π to be the column vector (analogous to Π in equation 27) of R_u, R_V, R_Φ. Thus,

$$R_\Pi = \begin{bmatrix} R_u(\lambda, \phi, P) \\ R_V(\lambda, \phi, P) \\ R_\Phi(\lambda, \phi, P) \end{bmatrix} \tag{31}$$

R_Π can be projected onto the normal modes through an expression analogous to equation (29). Thus the full non-linear form of equations (5 - 8) can be written in normal mode form as

$$\dot{x}_n^k = - 2\Omega i\, \sigma_n^k\, x_n^k + R_n^k(X) \tag{32}$$

where

$$R_n^k(X) = \langle R_\Pi \cdot \hat{\Pi}_n^k \rangle \tag{33}$$

Note that since R_u, R_V, R_Φ are non-linear terms, R_n^k is therefore a function of all the normal mode expansion coefficients and not simply of x_n^k. Thus we write R_n^k as a function of the column vector X defined earlier. We can also write formally an equation for the vector of normal mode expansion coefficients.

$$\dot{X} = - 2\Omega i \, \Lambda_x \, X + R_x(X) \qquad (34)$$

where Λ_x is a diagonal matrix whose elements are the non-dimensional eigenfrequencies σ_n^k and $R_x(X)$ is a short-hand notation for the projection of the non-linear terms on each of the normal modes in turn.

Equation (34) is a symbolic equation and would have the same form, no matter what the original model equations had been.

11. FAST AND SLOW EQUATIONS

The next step is to divide the set of normal modes up into fast modes and slow modes on the basis of their frequency. For many applications, it would be sufficient to define the fast modes simply to be the set of all gravity modes and the slow modes to be the set of all Rossby modes. Other applications require a more subtle distinction between fast and slow modes.

We will refer to the set of fast modes as Z and the set of slow modes as Y. Thus $X = Z + Y$. We can then re-write the normal mode form of the equation (34) in terms of a fast equation and a slow equation.

$$\dot{Z} = - 2\Omega i \, \Lambda_Z \, Z + R_Z(Z, Y) \qquad (35)$$

$$\dot{Y} = - 2\Omega i \, \Lambda_Y \, Y + R_Y(Z, Y) \qquad (36)$$

The non-linear projection onto the fast modes R_Z is a function of both fast and slow modes, and similarly for R_Y. In general, the frequencies Λ_Y are small compared with the frequencies Λ_Z.

12. LINEAR INITIALIZATION

We are now ready to consider the initialization problem. Suppose the model equations were the linearized form of equations (5 - 8), i.e. with $R_u = R_v = R_\Phi = 0$. Suppose we wish to eliminate high frequency oscillations (which we identify with the fast modes Z) from the model integration. The fast equation for this model, then, is

$$\dot{Z} = - 2\Omega i \, \Lambda_Z \, Z.$$

To eliminate fast oscillations for all time, it suffices at initial time to set

$$Z = 0. \tag{37}$$

However, if we have the full non-linear equations (R_u, R_v, $R_\Phi \neq 0$) then the appropriate fast equation is equation (35). In this case, setting $Z = 0$ at $t = 0$ will not suppress fast oscillations for all time as they will be re-excited by the non-linear term R_Z. This linear procedure was applied to the non-linear shallow water equations by Williamson (1976) and it was not capable of eliminating the fast oscillations.

13. NON-LINEAR INITIALIZATION - MACHENHAUER'S SCHEME

In an experiment performed with the non-linear shallow water equations, Machenhauer (1977) plotted separately the linear and non-linear contributions to the time tendencies of particular fast modes during the integration of the model. Thus, for a particular fast mode z from the set Z he would plot $2\Omega i\, \sigma_z\, z$ and $R_z(Z, Y)$ as a function of time. We show in Figure 3 a slightly modified version of Machenhauer's (1977) result.

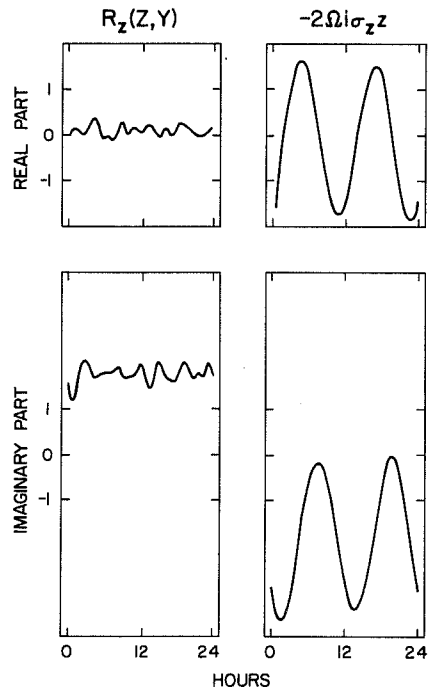

Figure 3 - after Machenhauer (1977)

In this diagram is shown the time behavior of a particular fast mode (the gravest gravity mode of zonal wavenumber 0). Both real and imaginary parts are shown. The curves on the left indicate the non-linear term while those on the right indicate the linear term. It can be seen that the linear oscillations are large, and in fact, have the same frequency as would be given by the linearized equations. The non-linear term, on the other hand, has only a very low amplitude high frequency oscillation.

Furthermore, in a time-averaged sense, the linear and non-linear terms nearly sum to zero.

This suggested to Machenhauer (1977) a scheme whereby the linear and non-linear terms would be balanced at initial time. This would be done by setting the initial time tendencies $\mathring{Z}$ in equation (35) equal to zero at time t = 0. This would give rise to a diagnostic equation which could be solved for Z. Note, however, that it is a non-linear equation in Z and requires iteration to convergence. Machenhauer's scheme does not change the slow modes Y. The scheme is as follows.

Step 1 is to apply linear initialization. The subscript indicates the iteration step.

$$Z_0 = 0, \quad Y_0 = Y \tag{38}$$

Step 2 is to set $\mathring{Z} = 0$ in equation (35)

$$Z_1 = \frac{R_Z(Z_0, Y_0)}{2\Omega i \, \Lambda_Z} \tag{39}$$

The next step is to repeat Step 2 except using Z_1 instead of Z_0. Thus

$$Z_2 = \frac{R_Z(Z_1, Y_0)}{2\Omega i \, \Lambda_Z} \tag{40}$$

This procedure would be repeated until convergence when the Z on the left hand side equalled the Z on the right hand side. The final values of the fast modes Z we will denote Z_B, where the subscript B stands for balanced. Thus

$$Z_B = \frac{R_Z(Z_B, Y_0)}{2\Omega i \, \Lambda_Z} \tag{41}$$

Now a non-linear iteration procedure such as this can only be expected to converge when the non-linear terms R_Z are small compared to the linear terms. This will be the case when the frequencies Λ_Z are large compared to the slow mode frequencies Λ_Y. Situations where this is not the case will be covered later.

14. NON-LINEAR INITIALIZATION - THE BAER-TRIBBIA SCHEME

Completely independently of Machenhauer, Baer and Tribbia developed a non-linear normal mode initialization scheme. This work is covered in Baer (1977) and Baer and Tribbia (1978). See also Ballish (1979).

The initialization scheme of Baer and Tribbia is more complex and difficult to use in practice than that of Machenhauer. However, it is also more general and powerful than Machenhauer's scheme.

The normal mode form of the model equation (39) has been derived from the dimensional form of the model equations (1 - 3). The Baer-Tribbia methodology can be best understood by considering the non-dimensional form of the original model equations. Thus, if we had first non-dimensionalized equations (1 - 3) using appropriate length and time scales, equation (34) could be rewritten in the following form:

$$\frac{\partial X}{\partial t} = - 2\Omega i \, \Lambda_X \, X + \varepsilon \, R_X(X) \tag{42}$$

where ε is a parameter which describes the strength of the non-linearity in the system. If the original model equations had been the shallow water equations, for example, then ε would correspond to a Rossby number (ratio of the non-linear to the Coriolis terms). For the planetary scales ε is generally taken to be small $0(.1)$. The analogues of the fast and slow equations (35 and 36) using this non-dimensionalization are

$$\frac{\partial Z}{\partial t} = - 2\Omega i \, \Lambda_Z \, Z + \varepsilon \, R_Z(Z, Y) \tag{43}$$

$$\frac{\partial Y}{\partial t} = - 2\Omega i \, \varepsilon \, \Lambda_Y \, Y + \varepsilon \, R_Y(Z, Y) \tag{44}$$

In these equations, all variables are $0(1)$ except ε. Note that an ε appears in the linear part of equation (44) because the frequencies Λ_y and Λ_z are assumed here to be of order unity whereas in equations (35 and 36) they were not.

We assume Z and Y are expanded in a power series in ε. Thus

$$Z = Z_0 + Z_1 \varepsilon + Z_2 \varepsilon^2 \ldots$$
$$Y = Y_0 + Y_1 \varepsilon + Y_2 \varepsilon^2 \ldots \tag{45}$$

We also assume that local time changes $\frac{\partial}{\partial t}$ can be represented by the sum of local time changes due to a fast time scale τ and a slow time T, namely,

$$\frac{\partial}{\partial t} = \frac{\partial}{\partial \tau} + \varepsilon \frac{\partial}{\partial T} \tag{46}$$

We can now rephrase the initialization problem as follows. Without changing Y, how can we adjust Z at initial time, so that there are no fast time oscillations for all time. This requires that $\frac{\partial}{\partial \tau} = 0$.

We will omit the details of the analysis which can be seen in Baer (1977) and Baer and Tribbia (1978) and give the results directly. Thus to second order in ε, the Baer-Tribbia scheme gives

$$Z_0 = 0, \quad Y_0 = Y \tag{47}$$

$$Z_1 = \frac{R_Z(Z_0, Y_0)}{2\Omega i \Lambda_Z} \tag{48}$$

$$Z_2 = \frac{1}{2\Omega i \Lambda_Z} \left[R_Z(Z_1, Y_0) - \frac{\partial Z_1}{\partial T} \right] \tag{49}$$

where a small approximation has been made in the second term of equation (49).

The first pass is simply linear initialization. The second pass is equivalent to the second pass through Machenhauer's scheme. The third pass is similar to the third pass through Machenhauer's scheme except for the addition of an extra term. Machenhauer's scheme is therefore not consistent to second order in ε, as the neglected term $\frac{\partial Z_1}{\partial T}$ may be of the same order as the retained terms.

The practical difficulty with the Baer-Tribbia technique is in the evaluation of the term $\frac{\partial Z}{\partial T}1$ in equation (49). It is possible, however, to evaluate this term by differentiating equation (48) with respect to T and evaluating the result numerically (see Tribbia, 1979). Thus

$$\frac{\partial Z_1}{\partial T} = \frac{1}{2\Omega i\, \Lambda_Z} \lim_{\lambda \to 0} \left[\frac{R_Z(Y_0 + \lambda \frac{\partial Y_0}{\partial t}, Z_0) - R_Z(Y_0, Z_0)}{\lambda} \right] \qquad (50)$$

where $\frac{\partial Y}{\partial t}0$ is evaluated from equation (44). Ballish (1979) has shown that the inclusion of this extra term can be important under certain circumstances.

15. SOME SUCCESSES OF NON-LINEAR NORMAL MODE INITIALIZATION

We shall now demonstrate that non-linear normal mode initialization "works" and that the effort expended is justified. We shall concentrate on the application of the Machenhauer scheme (Section 13) to two baroclinic primitive equation models - the ECMWF model and the Canadian Operational Spectral Model. The results in this section are taken from Temperton and Williamson (1979) and Daley (1979).

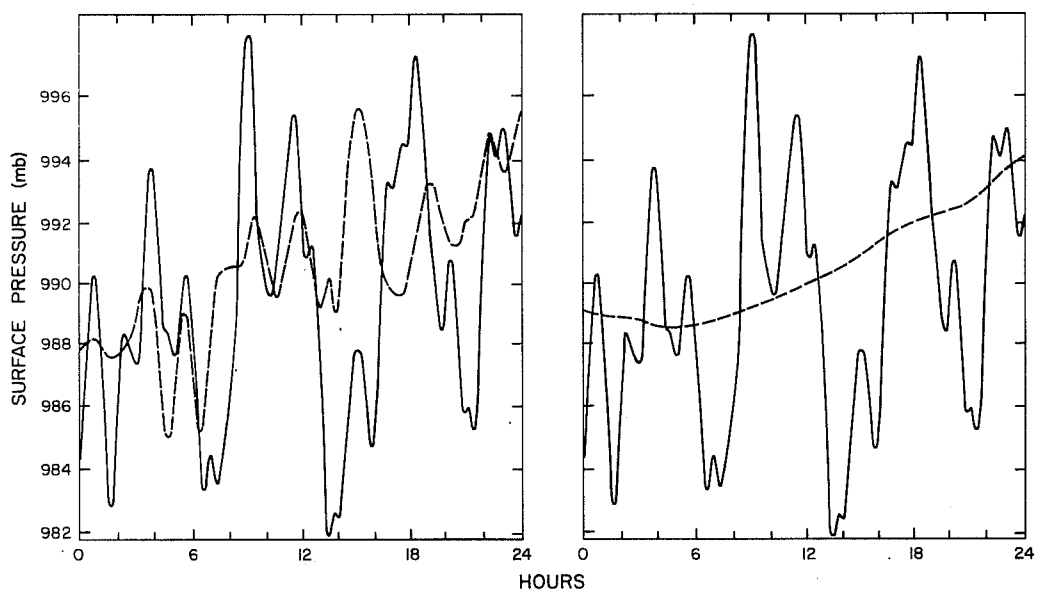

Figure 4 - after Temperton and Williamson (1979)

The acid test of any initialization scheme is - does it suppress high frequency gravity waves? We show in Figure 4 24-hour time traces of surface pressure at a particular gridpoint of the ECMWF model before and after linear and non-linear normal mode initialization. The solid lines (identical in both panels) indicate that without initialization there were high frequency oscillations of more than 10 millibars. The dashed line on the left panel indicates that linear initialization (Section 12) is only partially successful

in suppressing gravity waves. The dashed line on the right panel indicates the almost complete success of non-linear normal mode initialization in eliminating the high frequencies. To put this result in perspective, it should be stated that no other initialization scheme is capable of such success when applied to a model of the complexity of the ECMWF model.

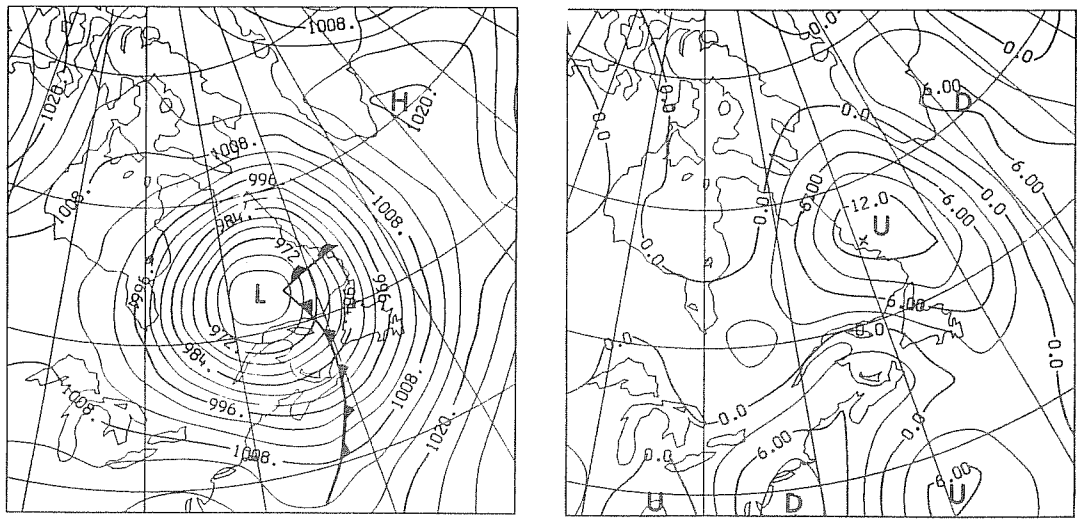

Figure 5 - after Daley (1979)

In addition to their ability to suppress high frequencies, initialization schemes are often required to provide consistent information to make up for deficiencies in the observation network. For example, it is difficult to accurately observe the divergent wind field or vertical motion, and the present initialization scheme has at least the possibility of providing this information. Figure 5 is taken from Daley (1979) and attempts to show the vertical motion field provided by the application of the Machenhauer scheme to the Canadian Operational Spectral Model. In the left panel is the surface pressure field and in the right panel is the 850 mb vertical motion field produced after non-linear initialization. The contours on the right panel are in mb/hr and U indicates upward motion while D indicates downward motion. It can be seen that the scheme produces upward motion ahead of the warm and cold fronts and downward motion behind the cold front, consistent with synoptic theory.

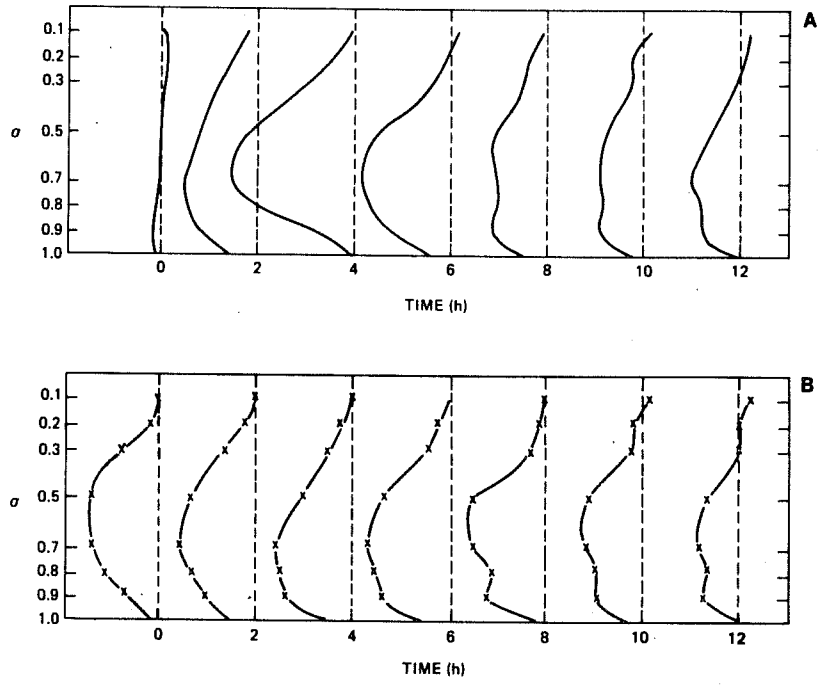

Figure 6 - after Daley (1979)

A second important question concerning the vertical motion field is: does it evolve slowly in time or does it oscillate before settling down? Figure 6 shows the vertical motion profiles as a function of time at the point marked X (Labrador Coast) on the right panel of Figure 5. The upper series is without initialization while the lower is with initialization. It can be seen that without initialization the vertical motion profile goes through an oscillation before settling down, while initialization produces a smoothly evolving sequence of profiles.

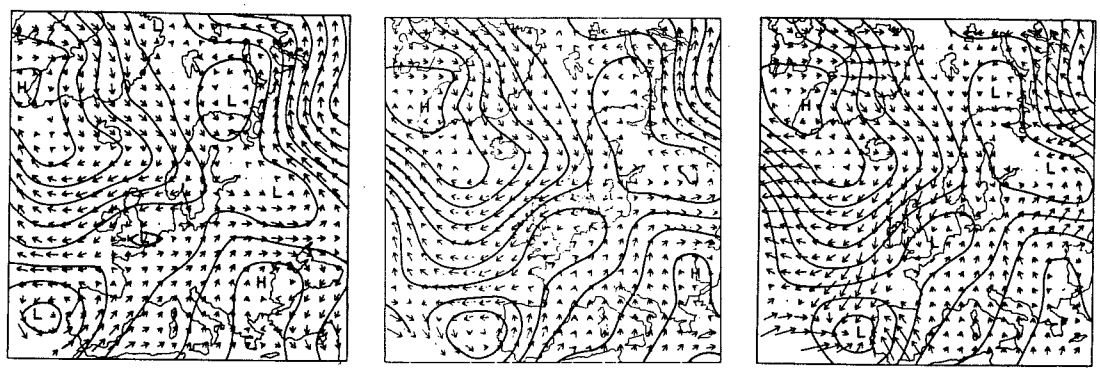

Figure 7 - after Temperton and Williamson (1979)

Non-linear normal mode initialization schemes are also capable of generating cross-isobar flow in the model boundary layer. Figure 7 is taken from Temperton and Williamson (1979). The left panel shows the 1000 mb geopotential height and winds without initialization. Note that the wind flow is more or less geostrophic. In the center panel is shown the same fields after application of the Machenhauer scheme to an adiabatic version of the ECMWF model. The flow has changed, but it is still more or less geostrophic. This is to be expected, because cross isobar flow in the boundary layer is a function of non-adiabatic terms such as the surface stress. The panel on the right shows the flow after application of the Machenhauer method to a version of the ECMWF model containing surface stress terms. Note the cross-isobar flow.

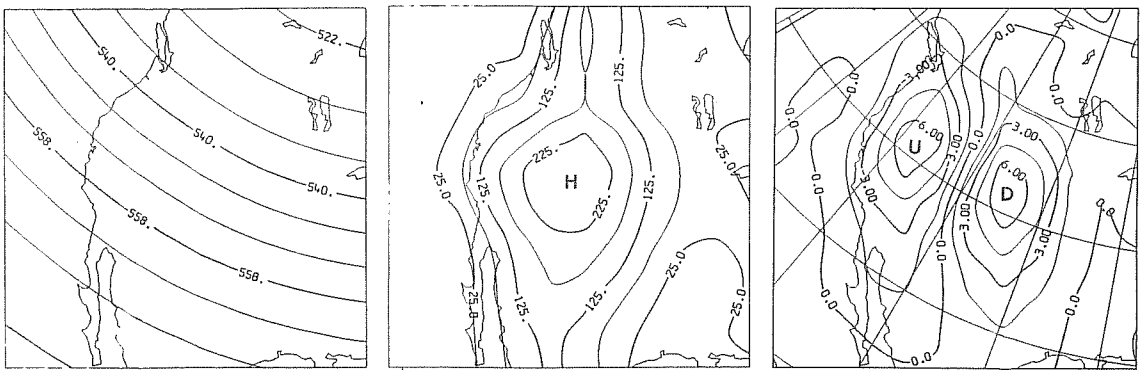

Figure 8 - after Daley (1979)

Non-linear normal mode initialization can also generate mountain induced vertical motion. There are some inconsistencies in the normal mode formulation in the presence of mountains (see Daley, 1979). Nonetheless, realistic terrain induced vertical motions can still be generated. Daley (1979) performed an experiment to demonstrate this. Since the terrain induced vertical motion is smaller in amplitude than the synoptic vertical motion, he started with idealized data in order to suppress the latter. An initially zonally averaged flow in pressure coordinates was interpolated to the terrain following coordinates of the Canadian Operational Spectral Model. Then Machenhauer's scheme was applied. In Figure 8, left hand panel, is shown the 500 mb geopotential height demonstrating the zonal averaging. In the center panel is shown the topography field of the Rocky

Mountain Range (dekameters) - the main axis of which is perpendicular to the flow. The right panel shows the resulting vertical motion (mb/hr). As hoped, the upstream vertical motion is upward (U) and the downstream vertical motion is downward (D).

The application of non-linear normal mode initialization is not without problems, however. These will be discussed in later sections.

16. THE SLOW MANIFOLD

Leith (1980) developed a graphical display which aids in the understanding of the initialization problem. The model normal modes can be represented in a multi-dimensional vector space. The Rossby and gravity modes each represent a subset or manifold of this vector space. In addition, Leith (1980) introduces the slow manifold which is defined to be the locus of all model states which are evolving slowly in time (i.e. have no fast time oscillations).

We can consider an approximation to the slow manifold by considering the locus of all points where $\dot{Z} = 0$ (equation 41). Figure 9, which is a modified version of Figure 1 of Leith (1980) is a simple two-dimensional illustration of the slow manifold concept. The amplitude of the Rossby modes Y is the abscissa while the gravity mode amplitude Z is the ordinate. The slow manifold M is the locus of all model states where $Z = Z_B$. As $(Z, Y) \rightarrow 0$ the non-linear terms $(R_Z, R_Y) \rightarrow 0$ and the slow manifold becomes coincident with the Rossby manifold.

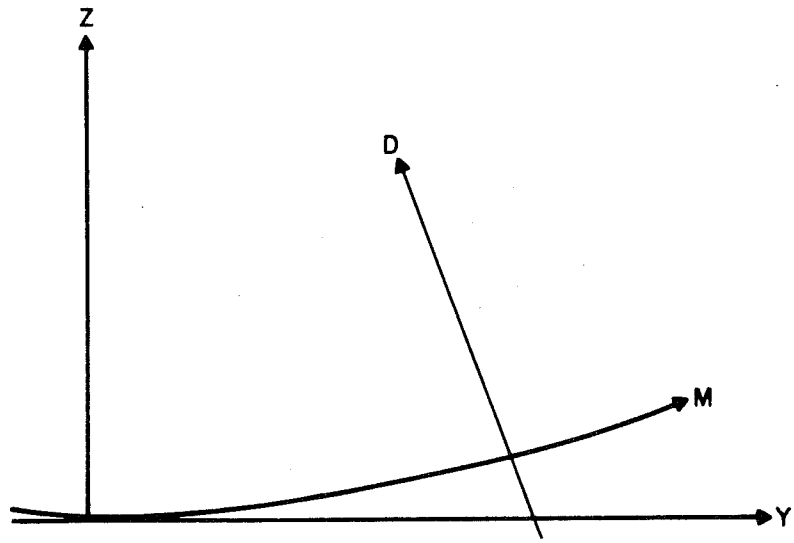

Figure 9 - after Leith (1980)

A particular point in this multi-dimensional space can have only a single spatial configuration for each of the dependent variables (geopotential, wind, etc.) of the model. Suppose, however, that the spatial structure of one of the model variables (geopotential, wind) were held fixed while the other variables were allowed to vary. The locus of model states which satisfy these conditions, Leith (1980) refers to as a data manifold. This manifold is indicated in Figure 9 by the line D.

The attractiveness of the slow manifold concept is that, in principle, it can be used to provide a visual interpretation of some problems in numerical weather prediction. The chief drawback is that for most models, the Rossby, gravity, slow and data manifolds cannot be visualized easily except in the schematic sense of Figure 9. One way around this dilemma is to define integrated manifolds as was done in Daley (1980). A second solution is to use a low order model in which the model variables have only 2 or 3 degrees of freedom. Tribbia (1980) developed such a model and we will examine his analysis in some detail.

17. THE GEOMETRY OF THE SLOW AND DATA MANIFOLDS

The model is of an isolated barotropic vortex on an f-plane. The radius of the vortex is b and the governing equations are the radically symmetric shallow-water equations

$$\begin{aligned}
&\frac{\partial u}{\partial t} + f_0 v = -\frac{1}{b}\left[v\frac{\partial u}{\partial r} + \frac{uv}{r}\right] \\
&\frac{\partial v}{\partial t} + f_0 u - \frac{1}{b}\frac{\partial \Phi}{\partial r} = -\frac{1}{b}\left[\frac{u^2}{r} - v\frac{\partial v}{\partial r}\right] \qquad (51) \\
&\frac{\partial \Phi}{\partial t} + \frac{g\tilde{H}}{br}\frac{\partial}{\partial r}\left[vr\right] = -\frac{1}{br}\left[\Phi vr\right]
\end{aligned}$$

where u, v are the tangential and radial velocity components, $\tilde{H}$ is the mean geopotential height of the free surface, r is a non-dimensional radial distance and f_0 is the (constant) Coriolis parameter.

We assume $u = U(t)\, J_1(\lambda r)$, $v = V(t)\, J_1(\lambda r)$, $\Phi = \Phi(t)\, J_0(\lambda r)$, where J_0, J_1 are Bessel functions of order 0, 1 and λ is the first root

of $J_1(r)$. The use of the Galerkin technique reduces equation (51) to the following set of ordinary differential equations.

$$\frac{\partial U}{\partial t} + f_o V = - \frac{UV}{b} I_1 \tag{52}$$

$$\frac{\partial V}{\partial t} - f_o U - \frac{\lambda \Phi}{b} = - \frac{1}{b} \left[V^2 I_2 - U^2 I_3 \right]$$

$$\frac{\partial \Phi}{\partial t} + \frac{\lambda g \tilde{H}}{b} V = - \frac{\Phi V}{b} I_4$$

where $I_1 - I_4$ are interaction coefficients (integrals of products of Bessel functions) defined in Tribbia (1980). For example,

$$I_3 = \int_0^1 J_1{}^3(\lambda r)\, dr \Big/\!\!\Big/ \int_0^1 r\, J_1{}^2(\lambda r)\, dr$$

The normal modes of the linearized version (left hand side) of equation (52) are found by assuming an exponential time behavior for U, V and Φ and inserting into the linearized equations. Thus

$$\begin{bmatrix} U \\ V \\ \Phi \end{bmatrix} = \begin{bmatrix} \hat{u} \\ i\hat{v} \\ f_o \hat{\Phi} \end{bmatrix} \exp(-i f_o \sigma t) \tag{53}$$

where σ is the non-dimensional frequency.

This gives rise to an algebraic eigenvalue problem of order 3 and there are thus 3 eigenvectors and corresponding eigenvalues. There is a Rossby mode with frequency $\sigma_R = 0$ and eigenstructure

$$\left[\hat{u}_R, \hat{v}_R, \hat{\Phi}_R \right] = \frac{1}{\sqrt{1 + K}} \left[- \lambda b^{-1}, 0, 1 \right] \tag{54}$$

and two gravity modes with frequency $\sigma_+ = \sqrt{1 + K}$ and $\sigma_- = - \sigma_+$ and eigenstructure

$$\left[\hat{u}_+, \hat{v}_+, \hat{\Phi}_+ \right] = \frac{1}{\sqrt{2(K-1)}} \left[\frac{\lambda b^{-1}}{\sqrt{K}}, \frac{\lambda b^{-1} \sqrt{K+1}}{\sqrt{K}}, \sqrt{K} \right] \tag{55}$$

where $\hat{u}_- = \hat{u}_+$, $\hat{v}_- = -\hat{v}_+$, $\hat{\Phi}_- = \hat{\Phi}_+$ and

$$K = \lambda^2 g\tilde{H} b^{-2} f_o^{-2} .$$

The normal modes have been orthonormalized, satisfying

$$c(\hat{u}_i \hat{u}_j + \hat{v}_i \hat{v}_j) + \hat{\Phi}_i \hat{\Phi}_j = \delta_j^i \tag{56}$$

where i, j indicates R, + or - and $c = g\tilde{H} f_o^{-2}$.

We can expand U, V, Φ as a linear combination of the three normal mode structures in analogy with equation (28)

$$\begin{bmatrix} U \\ V \\ \Phi \end{bmatrix} = \begin{pmatrix} \hat{u}_R & \hat{u}_+ & \hat{u}_- \\ \hat{v}_R & \hat{v}_+ & \hat{v}_- \\ \hat{\Phi}_R & \hat{\Phi}_+ & \hat{\Phi}_- \end{pmatrix} \begin{bmatrix} y \\ z_+ \\ z_- \end{bmatrix} \tag{57}$$

where y, z_+ and z_- are the expansion coefficients of the Rossby and gravity modes respectively. y, z_+ and z_- can be computed from (U, V, Φ) in analogy with equation (29)

$$\begin{bmatrix} y \\ z_+ \\ z_- \end{bmatrix} = \begin{pmatrix} c\hat{u}_R & c\hat{v}_R & \hat{\Phi}_R \\ c\hat{u}_+ & c\hat{v}_+ & \hat{\Phi}_+ \\ c\hat{u}_- & c\hat{v}_- & \hat{\Phi}_- \end{pmatrix} \begin{bmatrix} U \\ V \\ \Phi \end{bmatrix} . \tag{58}$$

Using these relationships, we can write the normal mode form of equation (52). We will write these equations formally in analogy with the slow and fast equations (35 and 36). The exact form of the equations can be seen in Tribbia (1980). Thus

$$\dot{y} = -i f_o \sigma_R y + R_y(y, z+, z-)$$

$$\dot{z}_+ = -i f_o \sigma_+ z_+ + R_+(y, z_+, z_-) \qquad (59)$$

$$\dot{z}_- = -i f_o \sigma_- z_- + R_-(y, z_+, z_-).$$

We can find the equation of the slow manifold by setting the time tendencies of all gravity modes equal to zero and finding the balancing components. In this case $\dot{z}_+ = \dot{z}_- = 0$. The resulting equation is analogous to equation (41). It is convenient to write these balanced equations, not in terms of y, z_+ and z_-, but in terms of the dependent variables U, V and Φ. In this form the equation of the slow manifold for this model is

$$V = 0$$

$$U^2 I_3 + \lambda\Phi + b f_o U = 0 \qquad (60)$$

Thus on the slow manifold of this model there is no radial velocity and the tangential wind satisfies a discretized form of the gradient wind equation.

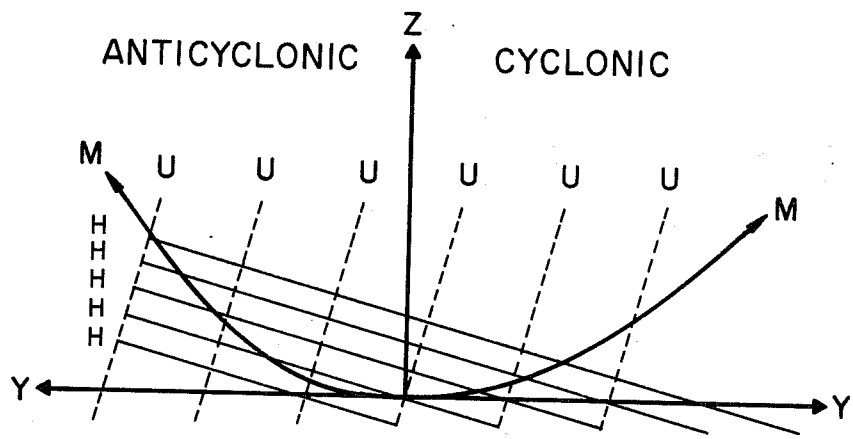

Figure 10 - after Daley (1980)

In Figure 10 (after Daley, 1980) is plotted the slow manifold diagram for this model. The abscissa is the amplitude of the Rossby mode y and the ordinate is the amplitude of the gravity mode z_+. (The diagram would look the same if z_- had been used instead.) In the present case, three parameters have to be specified. They are $\tilde{H}$ = 1 km, b = 1000 km and $f_o = f(45°)$. Solutions can be obtained for cyclonic and anticyclonic U. It is also possible to find the data manifolds for each of the variables U, V and Φ. Thus the dashed lines marked U are the U manifolds (U = constant) and similarly the solid lines marked H are the geopotential manifolds. The equation for the data manifolds are given by (57 and 58). We will define the data manifolds by the angle at which they intersect the Rossby axis (y) - the Rossby projection angle.

Figure 10 is really a projection on the y, z_+ plane of a three-dimensional space whose coordinates are y, z_+ and z_-. In fact U = constant is really a plane in this three-dimensional space. The direction cosine of a line normal to the plane U = constant with respect to the y (Rossby) axis is given by

$$\cos \beta_R^U = \frac{\hat{u}_R}{\sqrt{\hat{u}_R^2 + \hat{u}_+^2 + \hat{u}_-^2}}$$

where β_R^U is the direction cosine and superscript U represents the U data plane and subscript R represents the Rossby axis.

We will define the Rossby projection angle α_R^U to be the complement of β_R^U. Thus

$$\alpha_R^U = \Pi/2 - \beta_R^U \quad \text{and}$$

$$\sin^2 \alpha_R^U = \frac{\hat{u}_R^2}{\hat{u}_R^2 + \hat{u}_+^2 + \hat{u}_-^2} = \frac{K}{1+K} \tag{61}$$

from equations (54 and 55). Similarly it can be shown

$$\sin^2 \alpha_R^V = 0, \quad \sin^2 \alpha_R^\Phi = \frac{1}{1+K} \tag{62}$$

The expressions on the right hand sides of equations (61 and 62) are identical to those derived in geostrophic adjustment theory (Blumen, 1972). When K increases, α_R^U increases and α_R^Φ decreases. K is defined in equation (55) and it can be seen that α_R^U increases with decreasing horizontal scale, increasing vertical scale and decreasing latitude. α_R^Φ, on the other hand, increases with increasing horizontal scale, decreasing vertical scale and increasing latitude.

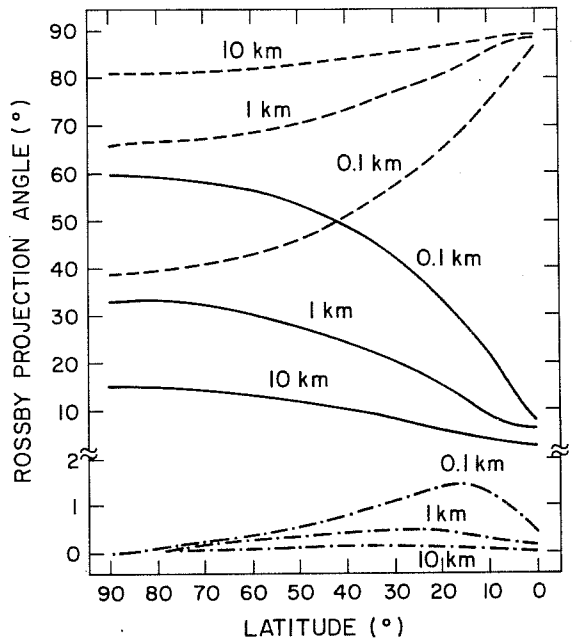

Figure 11 - after Daley (1980)

We see in Figure 11 the Rossby projection angle plotted as a function of latitude for three variables: geopotential (——), rotational wind component (— — —), divergent wind component (—•—), and 3 equivalent depths (10 km, 1 km, .1 km). These calculations are taken from Daley (1980) and apply to spherical geometry. The horizontal scale is fixed at 1000 km. Variations of Rossby projection angle on the sphere as a function of horizontal scale can be seen in Daley (1980).

18. CONSTRAINED INITIALIZATION

The initialization procedures we have described up to this point (both Machenhauer and Baer-Tribbia formulations) can be characterized as unconstrained initialization procedures. We will now consider

another class of initialization techniques, which will be referred to as constrained initialization procedures.

The concept of the slow manifold is very useful in graphically illustrating these different types of initialization procedures. Figure 12 is a schematic slow manifold diagram which will be used to illustrate constrained and unconstrained initialization. The Rossby manifold Y, slow manifold M, gravity manifold Z, and data manifold D are as in Figure 9.

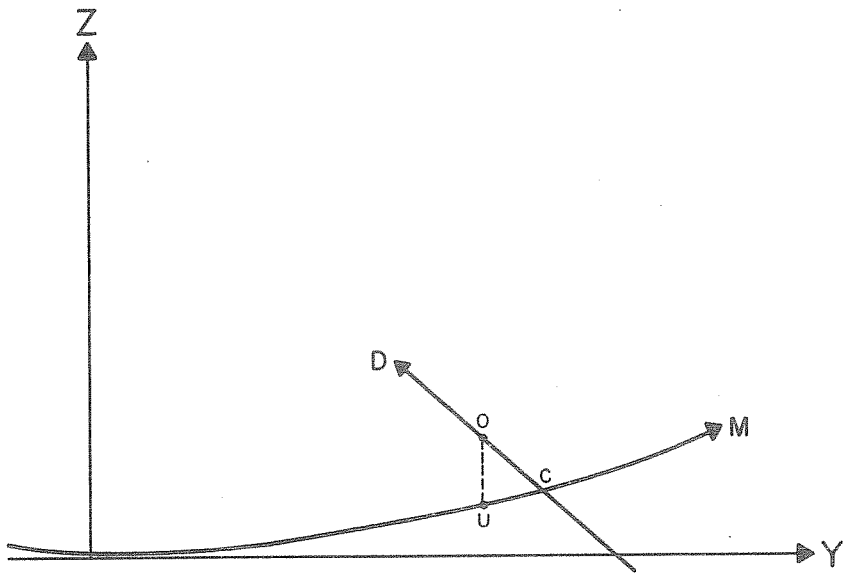

Figure 12

Suppose we have a model state at point 0 which lies on a data manifold D. We note that this point does not lie on the slow manifold, so that if used as an initial state for the model, gravity waves of magnitude proportional to the distance of 0 from M would be excited.

Now if we apply the unconstrained Machenhauer or Baer-Tribbia schemes discussed earlier, we can find an initial state on the slow manifold which will not excite gravity waves. In these schemes, it is assumed that the Rossby mode projection Y remains fixed. This corresponds to finding the point U (unconstrained) which is the intersection of the slow manifold and a vertical straight line passing through 0.

To fix ideas, let us suppose that the data manifold D is a geopotential manifold (i.e. the spatial structure of the geopotential field would be invariant along the line D). Furthermore, we suppose that our observations of the geopotential are everywhere very accurate, but that our wind observations are very poor. If we performed unconstrained initialization, thus arriving at the point U, the original geopotential data would no longer be fitted. Since we had great faith in our original geopotential observations, our initialized state (U) would clearly be unsatisfactory.

A much more reasonable initial state could be obtained by finding the intersection of the data manifold D and the slow manifold M. In the present case, this would imply that the original geopotential observations were fitted and yet no high frequencies would be excited in subsequent model integrations. This state is indicated by the point C (constrained) in Figure 12. This type of initialization would be referred to as geopotential constrained non-linear normal mode initialization.

In practice we have observations of both mass and wind, irregular in space and time and with varying accuracies. Some of the data will be inconsistent with other data, so we cannot expect to fit all data and still be on the slow manifold. However, we might have more faith in some observations than others, so we might desire that the adjusted state (a) be on the slow manifold and (b) fit the good data as well as possible and fit the poor data less exactly.

The operational solution of this problem is very complex, because it lies at the ill-defined interface between analysis (which attempts to fit the data according to its presumed accuracy) and initialization (which attempts to suppress high frequency oscillations).

Formally, however, one can write solutions to the constrained initialization problem using the variational calculus. Daley (1978) developed the variational formalism for the constrained normal mode initialization of the shallow water equations and solved it for some simple cases. The variational problem can be posed as follows.

Consider the case where we have observations of the vector wind $\underline{v}$ and geopotential Φ and we indicate our confidence in the observations

by means of weight functions $w_{\underline{v}}(\lambda, \phi, P)$, $w_{\Phi}(\lambda, \phi, P)$. Thus, where we had complete confidence in Φ, but none in $\underline{v}$, w_{Φ} would be large and $w_{\underline{v}} = 0$. This would correspond to remaining on a geopotential manifold. Conversely, $w_{\Phi} = 0$, $w_{\underline{v}}$ large would correspond to remaining on a wind manifold. The general solution, with both w_{Φ}, $w_{\underline{v}}$ nonzero would define a manifold somewhere in between the geopotential and wind manifolds. We can pose the general problem of going from model state 0 to model state c in Figure 12 as the minimization of the following functional

$$I = \int_A \left[(\underline{v}_o - \underline{v}_c)^2 \, w_{\underline{v}} + (\Phi_0 - \Phi_c)^2 \, w_{\Phi} \right] dA \tag{63}$$

where $\int_A [\ ]\, dA$ is an integral over the atmosphere, $\underline{v}_0, \Phi_0$ indicate the observed values and $\underline{v}_c$, Φ_c indicate the values after constrained initialization.

In the variational formulation we wish to minimize (63) subject to the constraint that the final state lie on the slow manifold. We can do this approximately by demanding that the final state satisfy Machenhauer's condition (41) - viz.

$$Z_c = \frac{R_Z(Z_c, Y_c)}{2\Omega i \, \Lambda_Z} \tag{64}$$

where Y_c and Z_c are the projection of the Rossby and gravity modes respectively after adjustment has taken place. Constraint (64) can be applied to the functional (63) by means of Lagrange's Undetermined Multipliers. This new functional is then minimized, leading to a set of Euler-Lagrange equations. We note that the projection on the Rossby modes Y will change after a data constrained initialization procedure. Unconstrained initialization is a special case of constrained initialization with a particular choice of w_{Φ}, $w_{\underline{v}}$ (see Daley, 1978).

Tribbia's (1980) approach to the variational problem is more elegant and direct than Daley's (1978) formulation, so we will sketch it briefly here. Tribbia's approach is iterative, with each iteration step containing 2 phases. The iteration procedure is shown schematically in Figure 13.

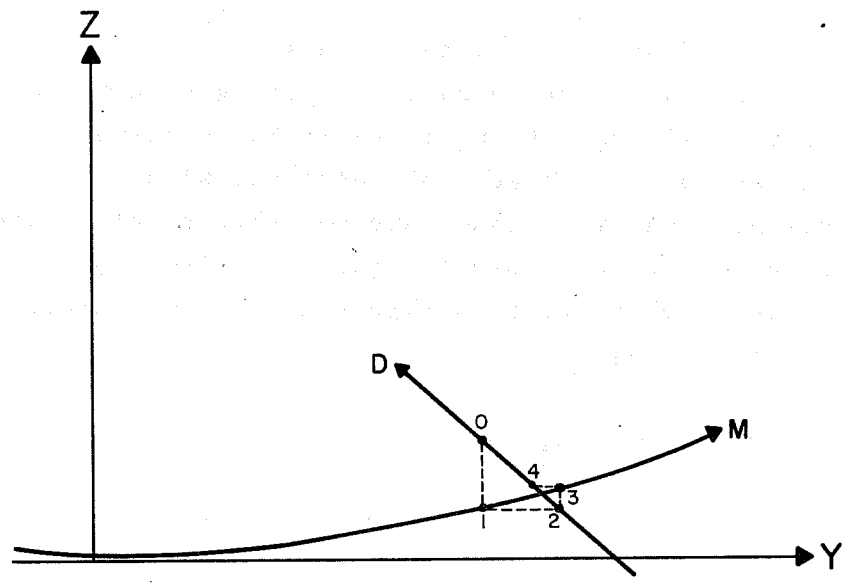

Figure 13

We assume that the initial observations are at point 0 as before. The first step is to use Machenhauer's unconstrained scheme to find point 1, which is on the slow manifold, but has the same Rossby projection as point 0. Thus

$$Z_1 = \frac{R_Z(Z_0, Y_0)}{2\Omega i \Lambda_Z} , \quad Y_1 = Y_0 \tag{65}$$

The next step is to get back on the data manifold at point 2. This is done by demanding that the projection on the gravity modes Z remain fixed while the projection on the Rossby manifold changes (horizontal straight line in Figure 13). This is the minimization part. We attempt to minimize the functional (63) with respect to the expansion coefficients of the Rossby modes. Thus

$$\frac{\partial I_{1,2}}{\partial y} = 0 \qquad \text{for all } y \in Y \tag{66}$$

where $I_{1,2} = \int_A \left[(\underline{v}_2 - \underline{v}_1)^2 w_{\underline{v}} + (\Phi_2 - \Phi_1)^2 w_\Phi \right] dA.$

Performing the minimization (66) will produce a series of linear algebraic equations in which the unknowns are the amplitudes of the Rossby modes Y at point 2.

We can then repeat step 1, arriving again at the slow manifold at point 3, and so on until convergence. The system of equations (65 and 66) is not difficult to solve if w_Φ and w_V are at most functions of latitude, but becomes more difficult when the weights have complete spatial variability (see Daley and Puri, 1980).

19. NON-LINEAR NORMAL MODE INITIALIZATION AND QUASI-GEOSTROPHIC THEORY

Leith (1980) showed the connection between non-linear normal mode initialization and quasi-geostrophic theory. He confined his attention to the first 2 passes through Machenhauer's scheme (equations 38 and 39). His analysis is fairly detailed and parts of it are similar to Section 17. Consequently, we shall omit many of the steps and concentrate on the results.

The analysis starts with the Boussinesq adiabatic equations on a f-plane

$$\frac{\partial u}{\partial t} - f_o v + \frac{\partial \Phi}{\partial x} = R_u \tag{67}$$

$$\frac{\partial v}{\partial t} + f_o u + \frac{\partial \Phi}{\partial y} = R_v \tag{68}$$

$$\frac{\partial s}{\partial t} + \frac{g}{\theta_o} \frac{\partial \theta^*}{\partial P} w = R_s \tag{69}$$

$$\frac{\partial u}{\partial x} + \frac{\partial v}{\partial y} + \frac{\partial w}{\partial z} = 0 \tag{70}$$

$$s = \frac{\partial \Phi}{\partial z} \tag{71}$$

where

$$R_{()} = - u \frac{\partial ()}{\partial x} - v \frac{\partial ()}{\partial y} - w \frac{\partial ()}{\partial z} \tag{72}$$

$$z = \frac{R \theta_o}{g \kappa} \left[1 - \left(\frac{P}{P_o} \right)^{\kappa} \right] \tag{73}$$

$$w = \frac{dz}{dt} \tag{74}$$

$$s = g \, \theta / \theta_o$$

P_o = pressure at bottom of atmosphere

θ = potential temperature

θ_o = horizontally and vertically averaged θ

θ^* = horizontally averaged θ

$\kappa = R/c_p$

These equations correspond exactly to the pressure coordinate equations (1 - 4) except for a minor approximation in the continuity equation (70) near the top of the atmosphere. z is a pseudo-height, which is close to the true height near the bottom of the atmosphere. It can be seen from equation (73) that at P = 0, $z = R\theta_o/g\kappa \simeq 28$ km.

To determine the normal modes, we proceed as in Section 17. We first linearize the equations about a basic state at rest, with a static stability profile $\theta^*(z)$ given by $N^2 = \frac{g}{\theta_o}\frac{\partial\theta^*}{\partial z}$ = constant. We then set $R_u = R_v = R_s = 0$ and assume that the dependent variables are represented by harmonic solutions in x, y, z, t.

$$\begin{bmatrix} u \\ v \\ s \end{bmatrix} = \begin{bmatrix} \hat{U} \\ \hat{V} \\ N\hat{S} \end{bmatrix} \exp i\left[n f_o N^{-1}(\lambda x + \mu y) + nz + f_o \sigma t\right] \qquad (75)$$

where λ, μ and n are the x, y and z wavenumbers and σ is non-dimensional frequency. This procedure leads to a set of algebraic eigenvalue problems of order 3 - one for each value of λ, μ or n.

There are 3 eigenvectors and corresponding eigenfrequencies, 1 Rossby mode and 2 gravity modes. The eigenfrequency of the Rossby mode is $\sigma_R = 0$, while the eigenfrequencies for the gravity modes are $\sigma_+ = \sqrt{1 + \mu^2 + \lambda^2}$ and $\sigma_- = -\sigma_+$. The eigenstructure of the Rossby mode is

$$[\hat{u}_R,\ \hat{v}_R,\ \hat{s}_R] = (1 + \mu^2 + \lambda^2)^{-\frac{1}{2}} [-\mu,\ \lambda,\ 1] \tag{76}$$

and similar expressions can be derived for the gravity modes.

We will define y, z_+ and z_- (in the same notation as Section 17) to be the values of the expansion coefficients for the Rossby and gravity modes before initialization commences. The first pass through Machenhauer's scheme produces new values of the normal mode expansion coefficients y(0), $z_+(0)$, $z_-(0)$ and the second pass produces y(1), $z_+(1)$, $z_-(1)$ etc. Corresponding to y, z_+, z_- are corresponding dependent variables u, v, s and their space discretized form (equation 75) - U, V, S.

The first pass through Machenhauer's procedure (equation 38) gives

$$z_+(0) = 0, \quad z_-(0) = 0, \quad y(0) = y.$$

We can calculate y from U, V, S by using the analogue of equation (58), viz.

$$y = \frac{1}{\sqrt{1 + \lambda^2 + \mu^2}} \left(- \mu U + \lambda V + S\right) \tag{77}$$

The values of U(0), V(0), S(0) can be obtained by using the analogue of equation (57) with $z_+ = z_- = 0$. Thus $U(0) = y(0)\ \hat{u}_R$, $V(0) = y(0)\hat{v}_R$, $S(0) = y(0)\ \hat{s}_R$. We can combine these two expressions together and obtain directly a relation between U(0), V(0), S(0) and U, V, S.

$$\begin{bmatrix} U(0) \\ V(0) \\ S(0) \end{bmatrix} = \frac{1}{\sqrt{1 + \mu^2 + \lambda^2}} \begin{pmatrix} \mu^2 & -\lambda\mu & -\mu \\ -\mu\lambda & \lambda^2 & \lambda \\ -\mu & \lambda & 1 \end{pmatrix} \begin{bmatrix} U \\ V \\ S \end{bmatrix}. \tag{78}$$

U(0), V(0), S(0) are the new values of the dependent variables obtained from the original values U, V, S after the first pass through Machenhauer's scheme.

From the eigenstructure of the Rossby mode (76) it is easy to see that $U(0) = -\mu\ S(0)$, $V(0) = \lambda\ S(0)$ and $\lambda\ U(0) + \mu\ V(0) = 0$. In real space form using equation (75) these relationships correspond to

$$f_o\, u(0) = -\frac{\partial \Phi(0)}{\partial x}, \quad f_o v(0) = \frac{\partial \Phi(0)}{\partial y}$$

$$\frac{\partial u(0)}{\partial x} + \frac{\partial v(0)}{\partial y} = 0, \quad w(0) = 0 \tag{79}$$

which are the f-plane geostrophic relationships.

It is also convenient to define a vorticity ξ and streamfunction ψ

$$\nabla^2\psi(0) = \xi(0) = \frac{\partial v(0)}{\partial x} - \frac{\partial u(0)}{\partial y} = \frac{1}{f_o}\ \nabla^2\Phi(0) \tag{80}$$

Thus the first pass through Machenhauer's scheme corresponds to geostrophic initialization for this simple model.

The second pass through Machenhauer's procedure (equation 34) can be written formally as

$$y(1) = y(0) \qquad z_+(1) = \frac{R_+(y(0),\ 0,\ 0)}{i\ f_o\ \sigma_+}$$

$$z_-(1) = \frac{R_-(y(0),\ 0,\ 0)}{i\ f_o\ \sigma_-} \tag{81}$$

We will omit the details of this analysis and go directly to the real space form of equation (81), involving relationships between u(1), v(1), Φ(1), s(1) etc. Thus

$$N^2\ \nabla^2\ w(1) + f_o^2\ w_{zz}(1) = f_o \frac{\partial}{\partial z}\left[\underline{v}(0)\cdot\nabla\xi(0)\right] - \nabla^2\left[\underline{v}(0)\cdot\nabla s(0)\right] \tag{82}$$

$$N^2\ \nabla^2\ \xi(1) + f_o^2\ \xi_{zz}(1) = 2f_o^{-1}\frac{\partial^2}{\partial z^2}\left[\Phi^2_{xy}(0) - \Phi_{xx}(0)\ \Phi_{yy}(0)\right] \tag{83}$$

$$f_o^{-1}\left[\nabla^2\Phi(1) + f_o^{\,2}\ N^{-2}\ \Phi_{zz}(1)\right] = 2f_o^{-1}\left[\psi_{xx}(0)\ \psi_{yy}(0) - \psi^2_{xy}(0)\right] \tag{84}$$

$$\nabla^2\psi(1) = -\ f_o\ N^{-2}\ \Phi_{zz}(1) \tag{85}$$

Now u(1), v(1), w(1) etc. are to be interpreted as corrections to the values of u(0), v(0), w(0) etc. obtained from the first pass through Machenhauer's scheme. Thus at the end of 2 passes through Machenhauer's scheme the adjusted fields would be u = u(0) + u(1), v = v(0) + v(1), w = w(0) + w(1) etc.

Equation (82) is a form of the quasi-geostrophic ω equation with the two terms on the right hand side corresponding to the thermal and vorticity advection terms. This equation is linear in $w = w(1)$ with the right hand side forcing function being calculated from the geostrophic solutions of the first pass.

By adding $\nabla^2\psi(0)$ to both sides of equation (84) and using equation (85) we can write

$$\nabla^2\psi + 2 f_o^{-1}\left[\psi_{xx}(0)\, \psi_{yy}(0) - \psi_{xy}^2(0)\right] - f_o^{-1}\, \nabla^2\Phi = 0 \qquad (86)$$

where $\psi(0)$ is the value of the streamfunction after one pass through Machenhauer's scheme and ψ and Φ are the corresponding streamfunction and geopotential at the end of the second pass. Equation (86) will be recognized as a form of the classical non-linear balance equation.

Normally, the non-linear balance equation is either solved for ψ given Φ (the forward direction) or solved for Φ given ψ (the reverse direction). In the former case with Φ specified - equation (86) would correspond to determining a first guess of the streamfunction $\psi(0)$ - equation (80) followed by the evaluation of the non-linear terms using $\psi(0)$ and then obtaining a new value of ψ from equation (86). In the reverse direction ψ is specified so $\psi(0) = \psi$ amd $\psi(1) = 0$, which leads to the much simpler problem of solving a Poisson equation for Φ.

In Machenhauer's unconstrained scheme there is no explicit direction of solution for equation (86). We note, however, that when the Rossby projection angle is large (near 90°) for the streamfunction then unconstrained initialization and streamfunction (or rotational wind component) constrained initialization become almost the same. From Section 17, this is likely to happen at large equivalent depth.

Thus, in the unconstrained situation, we are solving equation (86) in the reverse direction for large equivalent depth. Conversely, for small equivalent depth there would be a tendency to solve equation (86) in the forward (more difficult) direction.

20. SOME OUTSTANDING PROBLEMS WITH NON-LINEAR NORMAL MODE INITIALIZATION

We will now examine four problems with the non-linear normal mode initialization procedure. They are: (1) frequency separation in the tropics, (2) non-convergence in elliptic regions, (3) non-convergence for small equivalent depths, (4) disappointing initial rainfall rates.

20.1 Frequency separation in the tropics

Table 1 shows the clear separation in frequency between Rossby and gravity modes of the same equivalent depth. For tropically trapped modes, the separation is not so well defined and it is not clear whether or not non-linear normal mode initialization will be effective.

Tribbia (1979) examined this problem using an equatorial beta plane shallow water model. A model of this type is a reasonably good approximation to a spherical shallow water model in the ultra-long waves.

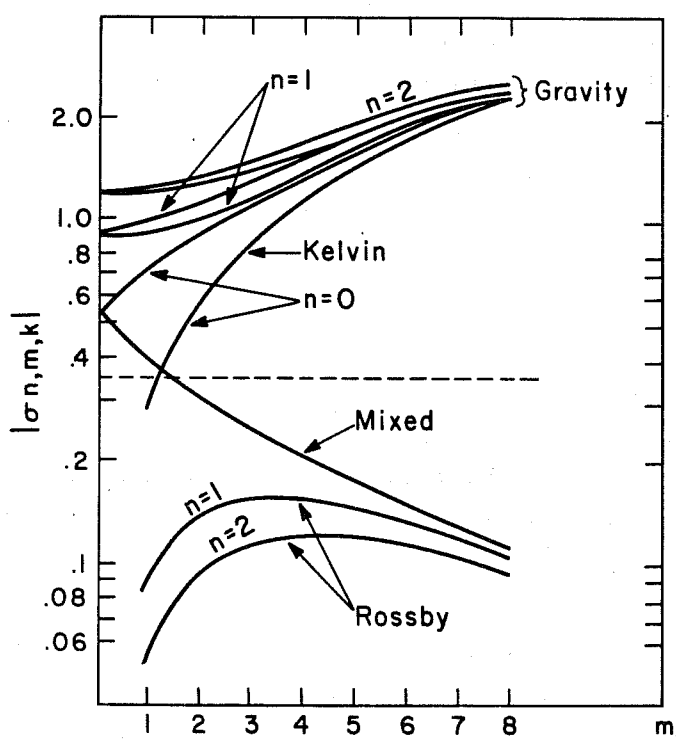

Figure 14 - after Tribbia (1979)

Figure 14 (from Tribbia, 1979) shows the non-dimensional frequency (σ) of the model normal modes as a function of zonal wavenumber m for an equivalent depth of 8 km. The meridional wavenumber n is indicated on the diagram. It can be seen that there is reasonably good separation between Rossby and gravity modes except for zonal wavenumbers 1 and 2. At these wavelengths the frequencies of the mixed Rossby-gravity waves (gravest anti-symmetric Rossby mode) and Kelvin wave (gravest eastward symmetric gravity mode) have similar magnitudes.

Tribbia (1979) decided to choose an arbitrary frequency (indicated by the horizontal dashed line in Figure 14) to separate the slow (Rossby) and fast (gravity) modes. He then initialized a non-linear equatorial beta plane model using the second order Baer-Tribbia scheme. The results of an integration are shown in Figure 15. The amplitude of a particular high frequency gravity mode is plotted for 24 hours during the integration of the model. The dashed curve is the integration corresponding to the initialization of equation (47) (linear), the dotted curve to equation (48) (first order Baer-Tribbia) and the solid curve to equation (49) (second order Baer-Tribbia).

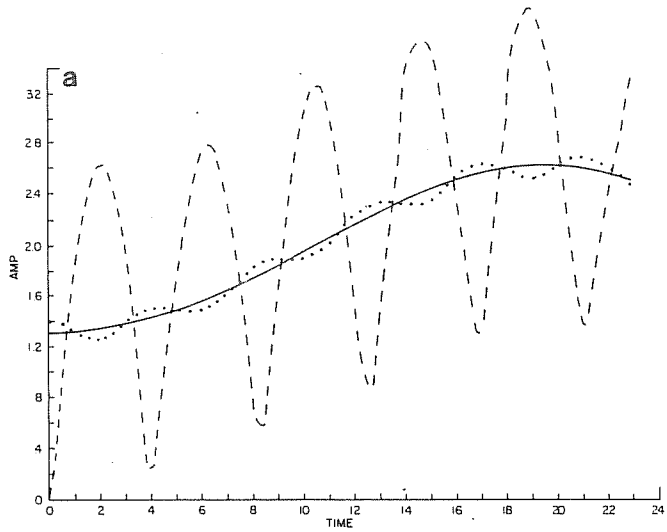

Figure 15 - after Tribbia (1979)

It can be seen that despite the relatively poor frequency separation, the Baer-Tribbia scheme works quite well.

20.2 Non-convergence in elliptic regions

Daley (1978) discovered that geopotential constrained Machenhauer initialization for the spherical non-linear shallow water equations did not converge. The regions of non-convergence coincided with the so-called non-elliptic regions where the classical non-linear balance equations (with geopotential specified) would not converge ($\nabla^2\Phi + 2f^2 < 0$).

Tribbia (1980) posed the question as to whether this apparent non-convergence was due to a numerical problem associated with the non-linear iterative scheme or whether, in fact, there was no solution at all under certain conditions.

Tribbia (1980) first constructed the simple isolated barotropic vortex model described in Section 17. It will be noted that in the slow manifold diagram for this model (Figure 10) there are certain geopotential data manifolds on the anti-cyclonic side which do not intersect the slow manifold. On the other hand, for any given U (tangential wind) manifold, there is always an intersection with the slow manifold. For any geopotential manifolds which do not intersect the slow manifold, no slowly varying solution is possible, gravity waves will always be excited.

Tribbia (1980) was first able to show that non-convergence of geopotential constrained initialization in elliptic regions was <u>not</u> due to faulty numerical iteration procedures. This was done as follows. The model in Section 17 has an analytic solution for the slow and data manifolds. However, Tribbia applied directly the constrained initialization procedures of Section 18 to this model and kept on iterating until he either got convergence or the solution started to diverge. Convergence was obtained for all geopotential manifolds which intersected the slow manifold (as indicated by the analytic solution), but there was no convergence for geopotential manifolds which did not intersect the slow manifold. This suggested that non-convergence of geopotential constrained initialization was a fundamental and not a numerical problem.

Tribbia (1980) then repeated his experiments using a more realistic model. This was a spherical non-linear shallow water model in

which the initial geopotential perturbation was circular and local. The amplitude, horizontal and vertical scales and central latitude of this disturbance could be varied at will. In this way, by using geopotential constrained Machenhauer initialization, Tribbia was able to determine the critical geopotential amplitudes between convergence and non-convergence as a function of latitude and scale. These results could then be compared to the f-plane results.

In all cases there was a critical geopotential amplitude (positive) for which geopotential constrained Machenhauer initialization would not converge. It would appear, then, that there exist geopotential fields for which the shallow water equations have no slowly varying solution. In the atmosphere, however, tropical high pressure systems exist which violate the criterion and yet have relatively slow time behavior. From this we must conclude that there are forcing terms (latent heat release) which maintain these high pressure areas in the real atmosphere. Consequently, the slow manifolds of a shallow water model and the atmosphere are clearly different for the case of strong tropical anti-cyclones.

20.3 Non-convergence for small equivalent depths

Daley (1979) and Temperton and Williamson (1979) both noticed that in the application of the unconstrained Machenhauer scheme to baroclinic models, the scheme would not converge when applied to gravity modes of small equivalent depth. Furthermore, it has also been noted that the application of Machenhauer's scheme to the ECMWF model suppresses the Hadley Cell.

The decision as to which modes to initialize and which modes to leave unadjusted (i.e. the division between fast and slow modes) is very critical in a baroclinic model. This is because many of the gravity modes with small equivalent dpeth (see Table 1) are of rather low frequency. Both Daley (1979) and Temperton and Williamson (1979) chose to make the division purely on the basis of equivalent depth. That is, they initialized all gravity modes with equivalent depth greater than some pre-specified critical equivalent depth and left all other modes untouched.

Temperton and Williamson (1979) investigated this effect using the 15 level ECMWF baroclinic model. They computed a quantity (BAL) which measures the balance in the adjusted gravity modes. Thus

$$BAL = \sum_{Z} \left[\frac{\partial Z}{\partial t} \right]^2$$

This quantity (BAL) is an integrated measure of the time tendencies of the fast modes. With no initialization this quantity would be large, but if Machenhauer's scheme (38 - 41) worked perfectly, it would approach zero. In any case if Machenhauer's scheme is converging, BAL should decrease after each iteration step.

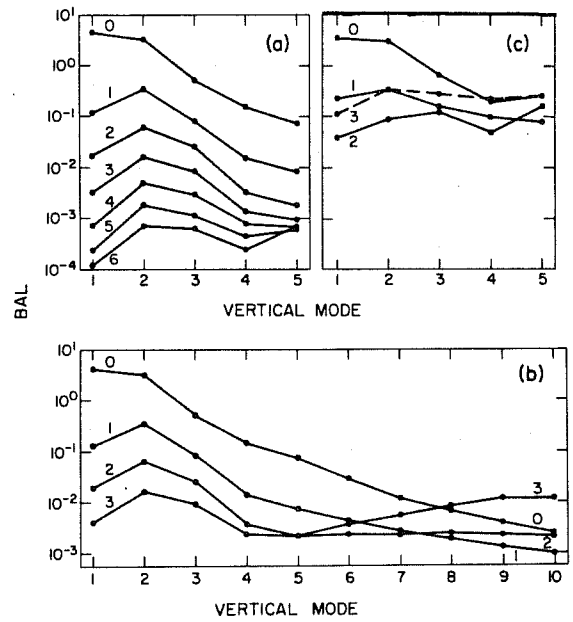

Figure 16 - after Temperton and Williamson (1979)

In Figure 16 BAL is plotted as a function of vertical mode number (external, first internal, etc.) for three different cases. The lines marked (0, 1, 2 ...) are the balance (BAL) as a function of iteration number. In Figure 16a BAL is plotted for the 15 level adiabatic version of the model in which the gravity modes for the 5 largest equivalent depths only have been adjusted. By and large, the scheme seems to be converging. Figure 16b is the same adiabatic case, but with the gravity modes corresponding to the first 10 equivalent depths adjusted. It can be seen that by the third pass, there is a diverging solution for small equivalent depths. Figure 16c is the same as Figure 16a except that the model is

non-adiabatic (i.e. includes parameterized radiation, convection, latent heat release etc.). It can be seen that even with only 5 modes, there is non-convergence in this case.

Why this should be so can be seen by examining equation (43). The scaling of equation (43) implicitly assumes that the frequency of the gravity modes Λ_Z is an order one quantity while the non-linear term $R_Z(Z, Y)$ has $\varepsilon << 1$ multiplying it. For small equivalent depth ε is no longer small. In this case the two terms on the right hand side of equation (43) might well be of the same order, in which case a non-linear iteration procedure such as Machenhauer's would not be likely to converge.

We will attempt a heuristic physical interpretation of this phenomena based on the f-plane quasi-geostrophic equivalent to Machenhauer's scheme developed in Section 19. We will consider equations (82 and 86) which are arrived at after the second pass through Machenhauer's scheme. Suppose that after many passes through Machenhauer's scheme, the equivalent equations to (86 and 82) are

$$\nabla^2\psi + 2f_o^{-1}\left[\psi_{xx}\,\psi_{yy} - \psi_{xy}^2\right] = f_o^{-1}\,\nabla^2\Phi \tag{87}$$

$$N^2\nabla^2 w + f_o^{\,2}\,w_{zz} = f_o\,\frac{\partial}{\partial z}\left[\underline{v}\cdot\nabla\xi\right] - \nabla^2\left[\underline{v}\cdot\nabla s\right]$$

$$+ NL(w) + F(w) \tag{88}$$

The first equation is a version of the non-linear balance equation, while the second is a version of the ω equation with the addition of two extra terms. NL(w) symbolically indicates non-linear terms in w or the divergent wind (the vertical advection of vorticity, for example) which do not appear in equation (82). F(w) symbolically indicates physical effects such as latent heat release which depend directly on w. Equations (87 and 88) have not been rigorously derived, but we are only interested in them as analogues to investigate the convergence process.

Consider first the balance equation (87). In Section 19 we suggested that for unconstrained initialization, at large equivalent depths this equation would essentially be solved in the reverse

direction (Φ from ψ), while for small equivalent depths it would be solved in the forward direction (ψ from Φ). Since the forward non-linear balance equation is much more difficult to solve, we might expect difficulties at small equivalent depths.

The real key to non-convergence at small equivalent depths probably lies in the ω equation (88). One pass through this equation with NL(w) = F(w) = 0 and the remaining right hand sides calculated geostrophically is equivalent to equation (82) and will yield a w field without any equivalent depth restriction. However, if w is calculated in this manner and then inserted into NL(w) and F(w) of equation (88) and an iteration attempted, it is not at all clear that a convergent solution will be obtained.

If we examine the vertical structure functions (Figure 1) we find that for very small equivalent depths there is more and more structure in the boundary layer. In the boundary layer, the normal free atmospheric scaling in which the divergent wind is much smaller than the rotational, is invalid. Consequently, for small equivalent depth NL(w) and F(w) might be quite large and equation (88) would not converge if solved iteratively.

There are practical remedies to this problem. Firstly, only for gravity modes with relatively high frequencies should Machenhauer's scheme be taken to convergence. Secondly, for gravity modes with lower frequencies, it might be desirable to take only 2 passes through the Machenhauer or Baer-Tribbia scheme, not for the purpose of suppressing rapid oscillations, but rather to provide consistent vertical motions on these scales.

20.4 Disappointing initial rainfall rates

Figures 5 and 6 show the non-linear normal mode initialization is capable of generating reasonable initial vertical motion fields with good time continuity. It is then reasonable to ask if the scheme can produce good initial precipitation rates. This question is raised because primitive equation models are notorious for their poor short-range precipitation forecasts.

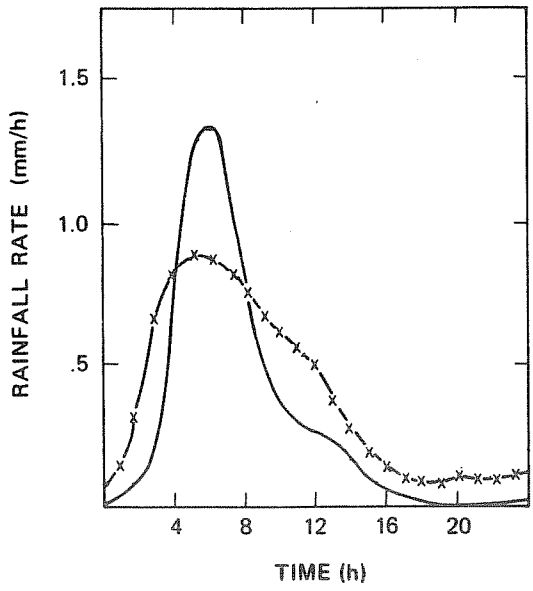

Figure 17 - after Daley (1979)

Figure 17 (from Daley, 1979) indicates that the short range precipitation problem cannot be solved by normal mode initialization alone. The solid line indicates the rainfall rate at the point x in Figure 5 without initialization. The x dash line in Figure 17 is the same except after initialization. It can be seen that the initialization scheme has suppressed the high frequencies, but has not made much improvement in the initial rainfall rate.

In order to get large rainfall rates, it is necessary that the vertical column be saturated as well as having a significant upward vertical motion. Since the initial upward vertical motion is large, it is the initial moisture analysis which must be deficient and must be modified before significant improvements can be expected in short-range precipitation forecasts.

21. RECENT DEVELOPMENTS AND RELATED RESEARCH

This review has concentrated on the use of model normal mode procedures in the initialization of primitive equation models. Recent work, however, suggests that the normal mode procedures have considerably wider application in numerical weather prediction. We will briefly discuss several of these more recent applications.

Daley and Puri (1980) have used normal mode procedures in an examination of the four-dimensional data assimilation problem. The

model normal modes were found to be particularly useful in diagnosing and partially ameliorating the data rejection problem.

Williamson, Daley and Schlatter* have examined optimal interpolation procedures using the model normal modes. They have shown that the geostrophic constraint used in multi-variate optimal interpolation procedures can both improve and degrade the analysis quality under certain conditions. Some experiments have been made with more realistic and general constraints than geostrophic.

Daley, Tribbia and Williamson* have examined the spurious excitation of large-scale external Rossby waves using the normal modes of barotropic and baroclinic models. In particular, it has been found that poor analysis methods in the tropics, or the imposition of an equatorial wall can excite spuriously large free Rossby modes. An attempt to initialize these modes using Machenhauer's technique was successful.

Normal mode methods are being used in more and more of the world's meteorological centers. We expect that these techniques will be used to gain understanding of the complex primitive equation models in use today and hopefully lead toward improvements in their performance.

References

Anderson, J., 1977: A routine for normal mode initialization with non-linear correction for a multi-level spectral model with triangular truncation. ECMWF Internal Report No. 15, 41 pp.

Baer, F., 1977: Adjustments of initial conditions required to suppress gravity oscillations in non-linear flows. Beitrage zur Physik der Atmosphäre, 50, 350-366.

Baer, F. and Tribbia, J., 1977: On complete filtering of gravity modes through non-linear initialization. Mon. Wea. Rev., 105, 1536-1539.

Ballish, B., 1979: Comparison of some non-linear initialization techniques. Preprint volume - Fourth Conference on Numerical Weather Prediction, Silver Spring, Maryland, October, 1979. 9-12.

---

* Paper in preparation.

Blumen, W., 1972: Geostrophic adjustment. Reviews of Geophysics and Space Physics, 10, 485-528.

Daley, R., 1978: Variational non-linear normal mode initialization. Tellus, 30, 201-218.

Daley, R., 1979: The application of non-linear normal mode initialization to an operational forecast model. Atmosphere-Ocean, 17, 97-124.

Daley, R., 1980: On the optimal specification of the initial state for deterministic forecasting. Accepted for publication in Mon. Wea. Rev.

Daley, R. and Puri, K., 1980: Four-dimensional data assimilation and the slow manifold. Mon. Wea. Rev., 108, 85-99.

Flattery, T., 1967: Hough functions. Technical Report No. 21, The University of Chicago, Department of the Geophysical Sciencies.

Flattery, T., 1970: Spectral models for global analysis and forecasting. Proc. Sixth AWS Technical Exchange Conference, U.S. Naval Academy, Air Weather Service Tech. Report 242, 42-53.

Hough, S., 1898: On the application of harmonic analysis to the dynamical theory of the tides - Part II. On the general integration of Laplace's dynamical equations. Phil. Trans. Roy. Soc. London, A191, 139-185.

Kasahara, A., 1976: Normal modes of ultra-long waves in the atmosphere. Mon. Wea. Rev., 104, 669-690.

Kasahara, A., 1978: Further studies on a spectral model of the global barotropic primitive equations with Hough harmonic expansions. J. Atmos. Sci., 35, 2043-2051.

Kasahara, A., 1980: Effect of zonal flows on the free oscillations of a barotropic atmosphere. J. Atmos. Sci., 37, 917-929.

Kasahara, A. and Puri, K., 1980: Spectral representation of three-dimensional global data by expansion in normal mode functions. NCAR manuscript 0501/79-8.

Leith, C., 1980: Non-linear normal mode initialization and quasi-geostrophic theory. J. Atmos. Sci., 37, 958-968.

Longuet-Higgins, M., 1968: The eigenfunctions of Laplace's tidal equations over a sphere. Phil. Trans. Roy. Soc. London, A262, 511-607.

Machenhauer, B., 1977: On the dynamics of gravity oscillations in a shallow water model, with applications to non-linear normal mode initialization. Beitrage zur Physik der Atmosphäre, 50, 253-271.

Taylor, G., 1936: The oscillations of the atmosphere. Proc. Roy. Soc. London, A156, 318-326.

Temperton, C. and Williamson, D., 1979: Normal mode initialization for a multi-level gridpoint model. ECMWF Technical Report No. 11, 99 pp.

Tribbia, J., 1979: Non-linear initialization on an equatorial beta plane. Mon. Wea. Rev., 107, 704-713.

Tribbia, J., 1980: Normal mode balancing and the ellipticity condition. Submitted to Mon. Wea. Rev.

Tribbia, J., 1980: A note on variational non-linear normal mode initialization. Submitted to Mon. Wea. Rev.

Williamson, D., 1976: Normal mode initialization procedure applied to forecasts with the global shallow water equations. Mon. Wea. Rev., 104, 195-206.

Williamson, D., and Dickinson, R., 1976: Free oscillations of the NCAR global circulation model. Mon. Wea. Rev., 104, 1372-1391.